PHILOSOPHICAL TRANSACTIONS OF THE ROYAL SOCIETY A MATHEMATICAL, PHYSICAL & ENGINEERING SCIENCES

An Experimental Determination of the Fermi Surface in Lead

A. V. Gold

Phil. Trans. R. Soc. Lond. A 1958 **251**, 85-112
doi: 10.1098/rsta.1958.0010

AN EXPERIMENTAL DETERMINATION OF THE FERMI SURFACE IN LEAD

By A. V. GOLD

The Royal Society Mond Laboratory, University of Cambridge

(*Communicated by D. Shoenberg, F.R.S.—Received* 29 *March* 1958)

[Plate 1]

CONTENTS

The oscillatory variation of magnetic moment with magnetic field (de Haas–van Alphen effect) has been studied in lead single crystals in the range 1·2 to 4·2°K and at fields up to 80 kG using an impulsive-field technique. The oscillations consist of several terms with periods ranging from $0{\cdot}53 \times 10^{-8}\,G^{-1}$ to $5{\cdot}4 \times 10^{-8}\,G^{-1}$. Particular attention has been paid to the variation of the periods with orientation of the field relative to crystal axes and the shape of the Fermi surface has been inferred from these results. The Fermi surface is found to consist of several pieces and application of the simple free-electron model has enabled these pieces to be fitted into the Brillouin zone scheme in a consistent manner. The surfaces found are (i) a sphere containing holes in the second zone, (ii) a multiply connected surface containing electrons in the third zone, and (iii) six 'cushion-shaped' surfaces containing electrons in the fourth zone. The volumes within the surfaces have been estimated, giving roughly 0·45 hole per atom in the second zone and 0·45 electron per atom in the third and fourth zones, and the interpretation is consistent with ascribing a total of four valence electrons per atom to lead. From the temperature dependence of the amplitudes of the oscillations, 'effective mass' values have been obtained; using these data and the dimensions of the various surfaces, an estimate has been made of the electronic specific heat constant γ and the probable form of the curve of density of states *against* energy is indicated. The proposed Fermi surface is shown to be reasonably consistent with other experimental evidence. The field and orientation dependence of the de Haas–van Alphen amplitudes are discussed and the experi-

mental amplitudes are compared with the theoretical amplitudes given by Lifshitz & Kosevich (1955); while the amplitudes of some of the oscillations are found to be considerably greater than those given by theory, others become unobservably small over large angular ranges. The de Haas–van Alphen effect has also been studied in dilute lead–bismuth alloys but no simple interpretation has been found for the observed changes in period.

1. Introduction

The de Haas–van Alphen effect (the oscillatory variation of magnetic moment with magnetic field in metal single crystals at low temperatures) has been observed in a considerable number of metals; a comprehensive review of both theory and experiment has been given by Shoenberg (1957). As was pointed out by Onsager (1952) and Lifshitz & Kosevich (1955), the period P of the oscillatory part of the diamagnetism of the conduction electrons is given by

$$P = \Delta(1/H) = 2\pi e/c\hbar\mathscr{A}_0, \tag{1}$$

where e, c and $\hbar$ have their usual meanings and $\mathscr{A}_0$ is an extreme (i.e. maximum or minimum) area of cross-section of the Fermi surface (in $\mathbf{k}$-space) by a plane normal to the magnetic field H, whatever the shape of the Fermi surface. If the Fermi surface consists of several pieces, the resulting oscillations should consist of a number of periodic terms superimposed on one another, one arising from each extreme area.

Since the extreme area of cross-section is related to the period of the de Haas–van Alphen oscillations by the simple inverse proportion (1), without recourse to any complicated averaging process, the de Haas–van Alphen effect is, in principle, a powerful tool for a study of the Fermi surface. A knowledge of the variation of $P(\theta,\phi)$, and hence $\mathscr{A}_0(\theta,\phi)$, with (θ,ϕ), the angles between the field and two appropriate crystallographic axes, should enable the shape of the surface to be determined. This can be done by a trial and error fitting or by a direct calculation using the procedure of Lifshitz & Pogorelov (1954) (which assumes, however, that the surface is centro-symmetric and that the extreme section is always the central section).

Further information about the energy surfaces may be obtained from the temperature dependence of the amplitudes of the oscillations; this gives the 'effective mass' m^* of the relevant carriers, where

$$m^* = (\hbar^2/2\pi)\,(\partial\mathscr{A}/\partial E)_0, \tag{2}$$

the derivative being taken at the Fermi level. Now the Fermi velocity $\mathbf{v}_0$ is given by $(1/\hbar)$ grad $_{\mathbf{k}}E$ at any point on the Fermi surface, so that, knowing the shape of the surface and the angular variation of $(\partial\mathscr{A}/\partial E)_0$, it should be possible to determine $\mathbf{v}_0$ for any orientation, though usually the data from the temperature dependence of amplitude is not complete enough to warrant a detailed calculation.

Previous studies of the anisotropy of period in various metals have been carried out at fields up to 30 kG, and it was found that the surfaces giving rise to these oscillations are made up of small 'pockets' containing few electrons or holes of low effective mass (between 10^{-3} and 10^{-2} carrier per atom). Examination of the theoretical expression for the amplitude given by Lifshitz & Kosevich (1955) shows that, for larger portions of the Fermi surface, where the carriers may be expected to have something like the normal electronic mass, fields of the order of 10^5 G are required to give an appreciable amplitude of oscillation; in addition, the resolution of short-period oscillations is improved at high fields.

This paper describes a detailed study of the de Haas–van Alphen effect in lead at fields up to 80 kG using an impulsive-field technique (Shoenberg 1953), and from these results a fairly complete picture of the band structure near the Fermi surface has been obtained. Preliminary investigations (Shoenberg 1953) had revealed oscillations of short period (corresponding to relatively large pieces of Fermi surface) in both lead and tin. Lead was chosen for this study since the oscillations appeared to be less complex than those in tin; furthermore, it was felt that the interpretation of the results would be easier for a metal with cubic symmetry.

A brief preliminary account of this work has already been reported (Gold 1957).

2. Experimental method

The method used is essentially that described by Shoenberg (1953, 1957) and only a brief account of the basic technique will be given here. However, some additional features, such as the mechanism for varying the angle between the field and crystal axes, have since been incorporated; these features and the procedure of period measurement will be described in rather more detail.

(*a*) *General principles*

Oscillations in differential susceptibility $\mathrm{d}I/\mathrm{d}H$ (I is the magnetic moment per unit volume) are detected as an e.m.f. induced in a pick-up coil surrounding a thin-wire specimen as the magnetic field is made to vary rapidly with time. The field is produced by discharging a 2000 μF condenser charged to 1700 V through a liquid-nitrogen cooled solenoid. In the design of the solenoid, the following considerations must be taken into account. In order to get high fields it is necessary to have a short discharge time; however, the field must not vary so rapidly as to induce eddy currents of appreciable magnitude in the specimen and a compromise between these two requirements must be arrived at. In addition, the field is required to be homogeneous to better than one part in 10^4 over a distance of 1 cm at the centre of the solenoid. The solenoid used gives a field pulse rising to a peak of 80 kG in 11 ms and consists of 2300 turns of 22 s.w.g. copper wire wound in sixteen layers on a thin former of internal diameter 15 mm and length 120 mm; the homogeneity is improved by suitably placed auxiliary windings. Inside a thin-walled liquid-helium Dewar vessel, which passes through the solenoid, are two similar pick-up coils, each of 800 turns of 46 s.w.g. wire, connected in series-opposition. One contains the specimen and the other serves to neutralize most of the e.m.f. induced by the field alone. The signal from the coils, at most a few millivolts in magnitude, is, after considerable amplification, made to appear as an oscillatory trace on one beam of a double-beam cathode-ray tube. The remaining out-of-balance voltage is of frequency low compared to the de Haas–van Alphen signal and is removed by a high-pass filter. By means of a variable delay and time-base any portion of the whole discharge may be selected, expanded at will on the screen and photographed. The field is measured by recording, on the second beam of the cathode-ray tube, the potential developed across a low resistance in series with the solenoid.

(*b*) *The specimens and the rotating mechanism*

The specimens are in the form of thin single crystal wires of diameter about $\frac{1}{2}$ mm and length about 6 mm; if much thicker wires were used the effects of eddy currents would become appreciable. The wires are extruded from Johnson–Matthey lead rods of purity

PHILOSOPHICAL TRANSACTIONS OF THE ROYAL SOCIETY A MATHEMATICAL, PHYSICAL & ENGINEERING SCIENCES

greater than 99·995 % lead (lab. no. 4138) and crystallized in any desired orientation (usually with [100] or [110] axes along the wire) by means of a seed crystal. The specimen is mounted inside a protective glass tube by a spot of Durofix cement at its tip and the tube is then glued into a short hollow ivory cylinder to which a small reference mirror has been attached. The orientation of crystal axes relative to the axis of the ivory cylinder and the normal to the mirror is determined from back-reflexion Laue photographs (the optical goniometer method using etch-pit reflexions cannot be used, since the reflexions are too faint when the specimen is mounted in the glass tube). The mounting is then fitted into one of the two pick-up coils, leaving the top of the cylinder and the mirror exposed.

To set the specimen in any desired orientation with respect to the fixed magnetic field, the two pick-up coils are mounted side by side inside an ivory wheel which can be rotated in ivory forks by strings passing up to a winch at the top of the cryostat.† Before a liquid-helium run the specimen mount is rotated about its own axis until a chosen crystallographic plane coincides with the plane of the wheel. This is done with the whole mechanism outside the cryostat, using the small reference mirror and a lamp-and-scale device. By this method the specimen can be set so that, when the wheel is rotated during a liquid-helium run, the field remains in the chosen crystallographic plane to within about 3°.

The angle between the field and the wire (i.e. between the field and some known crystallographic direction) is measured by means of a pointer attached to the winch at the top of the cryostat. However, as the liquid-helium level falls the reading of the pointer for a given setting drifts and consequently the readings become unreliable.This difficulty is overcome by feeding the solenoid with a 10 kc/s signal and measuring the e.m.f. induced in the pick-up coils; this e.m.f. varies smoothly with the angular position of the wheel, and, once calibrated at some constant level, can be used as a reference independent of the level. By this method angular differences can be measured accurately, but the zero reading (corresponding to zero angle between the field and the wire) can be deduced only indirectly from the symmetry of the period-orientation curves.

(*c*) *The oscillograms and measurement of period and amplitude*

Typical oscillograms obtained for the lead oscillations are shown in figure 1 (plate 1). The first three of these, *a*, *b* and *c*, show envelopes over a wide field range for different orientations. The field falls from nearly 80 kG (upper calibration line) to about 25 kG and it can be seen that the oscillatory e.m.f. induced in the pick-up coils vanishes, as it should, at the peak field where $dH/dt = 0$. The complex beat patterns indicate the presence of two or more components of slightly different periods and the faint lines running through these pictures at high fields are due to much faster oscillations of lower amplitude. From these pictures alone it can be seen that the Fermi surface must consist of several portions.

The period is measured by expanding a portion of the whole envelope until the oscillations are resolved and counting the number of cycles between two values of the field. Since the relative change in field corresponding to the largest number of cycles which can be conveniently resolved is seldom more than 10 % for the oscillations in lead, the accuracy

† It was found necessary to use Fluon bearings to avoid jamming at low temperatures. The choice of ivory was somewhat accidental; probably some other strong insulating material could have been used.

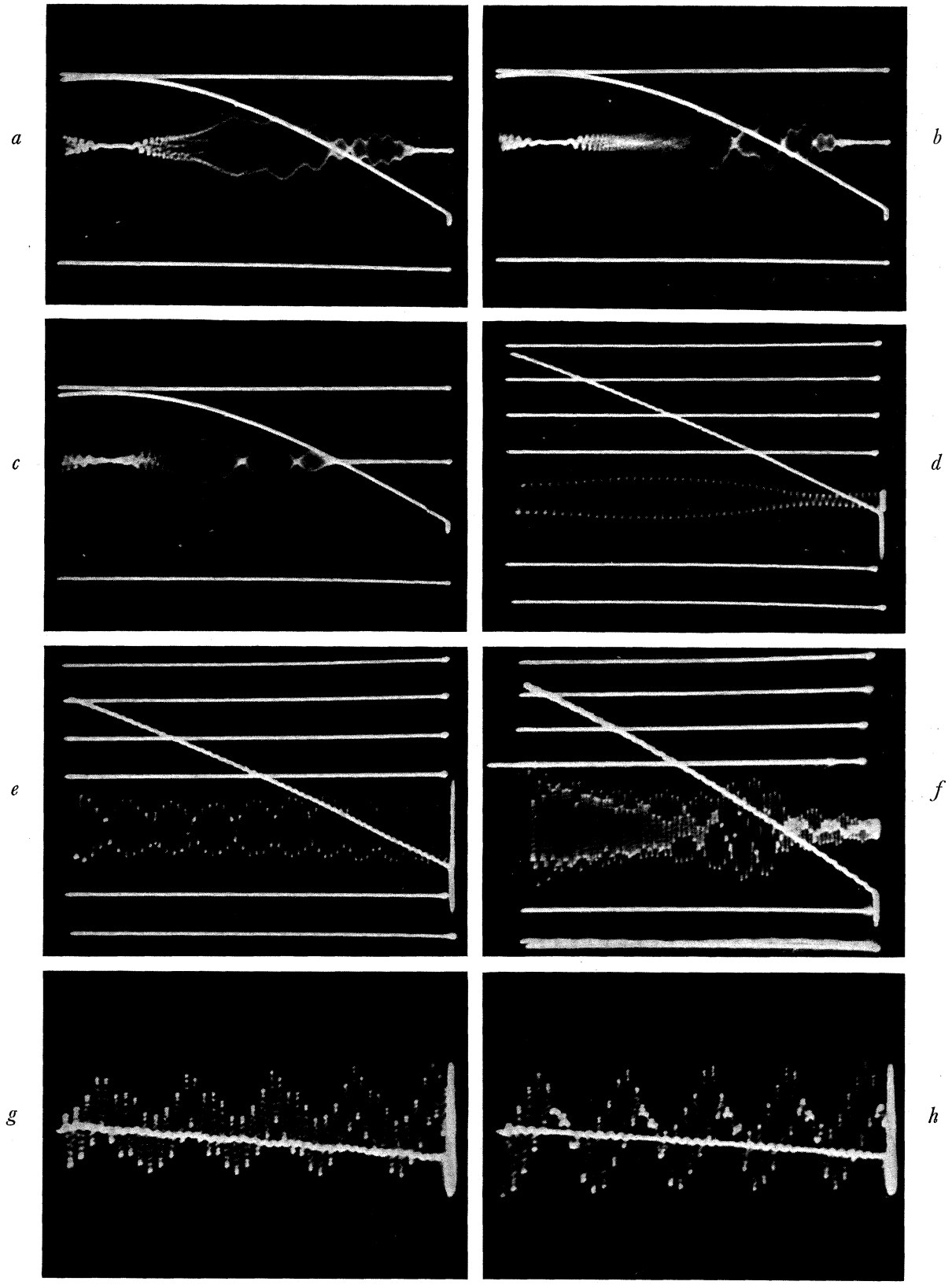

FIGURE 1. Typical oscillograms of lead oscillations. *a*, *b* and *c* are envelope pictures of the γ-oscillations at 30°, 40° and 45° from [100] in a (100) plane (i.e. *c* is at [110]). $T = 2{\cdot}3\,^{\circ}\mathrm{K}$; at $T = 1{\cdot}2\,^{\circ}\mathrm{K}$ the patterns extend to lower fields so that, for example, three more beats are observed at [110]. *a*, *b* and *c* show the field variation directly without using the 'back-off' technique; the sweep time is 15 ms and the horizontal calibration lines correspond to 0 and 80 kG. The remaining oscillograms are expanded pictures with sweep times from 0·5 to 1·5 ms. *d* and *e* show the γ-oscillations at two different orientations and *f* illustrates a resonance of group γ against a background of group β (at [100]); the calibration lines are at intervals of 1·57 kG and the baselines correspond to 44, 44 and 52 kG for *d*, *e* and *f*, respectively. *g* and *h* show the α-oscillations superimposed on the slower γ ones.

(*Facing p.* 88)

of a period determination depends very much on the accuracy of the determination of the change in field. The necessary accuracy is achieved by 'backing-off' most of the potential developed across the series resistance by an accurately known steady potential; the small difference is then greatly amplified and applied to the second beam of the cathode-ray tube. In addition, calibration lines are automatically photographed after each discharge to eliminate screen distortion and variations in the sensitivities of the difference-amplifier and of the tube. Figure 1*d* (plate 1) shows such an expanded picture suitable for period measurement (the calibration lines are at intervals of 1·57 kG and the lowest one corresponds to 44 kG). When fast oscillations are superimposed on slower ones as in figure 1*g* and *h*, the shorter period can best be determined by counting the number of cycles to each cycle of the longer one, which can be more accurately measured directly. In figure 1*e* are shown beats formed by two components with periods which differ by about 20%; for such beats the period of the dominant term was measured as before and the period difference was obtained from the beat period. Whether the subordinate term was of greater or lesser period than the dominant one could be decided by running a travelling microscope along the oscillations and measuring the distance between the peaks of the individual cycles; if this distance was always greatest at beat minima, then the subordinate term was of shorter period than the dominant one, and vice-versa.

By connecting a condenser across the pick-up coils it was possible to enhance the amplitude considerably whenever the time-frequency of the oscillatory e.m.f. was near the resonant frequency of the coil-condenser circuit. This was of great help in studying oscillations of low amplitude which would otherwise have been swamped by stronger oscillations of different period. The resonance of a low-amplitude term, whose period is about 2·2 times that of the dominant oscillations, is shown in figure 1*f* (plate 1). It will be noticed that the 'maxima' in the upper half of the envelope of the pattern coincide with the 'minima' in the lower half, a feature which occurs whenever the period of one of the terms is between two and three times that of the other.

In orientations where only one component was present, individual period determinations were usually within about 3% of the mean, but the accuracy was, of course, poorer when the oscillograms were more complex. For faster oscillations superimposed on slower ones the scatter of the short period determinations was as much as 8% about the mean. As a check on the absolute accuracy, period measurements were made on crystals of aluminium and tin for comparison with existing data on these metals obtained from the more direct torque method at low fields. For aluminium, the period along a [111] direction was about 10% shorter than that found by Gunnersen (1956). Similarly, the period for tin along a binary axis was about 10% shorter than that found by Shoenberg (1952), though it was in excellent agreement with that found by Berlincourt (1952). Although it is not clear whether the cause of the discrepancy lies in some unsuspected error in the present method or in the older data, it is probably wise not to rely on absolute values of period to better than 10%.

The absolute value of the amplitude, A, of the oscillations in $\mathrm{d}I/\mathrm{d}H$ can be estimated for any particular value of the field to within a factor of two or three from the magnitude of the oscillatory e.m.f., the number of turns in the pick-up coil and its orientation relative to the field, the specimen size and the rate of change of the field; corrections are applied when the amplitude of the e.m.f. has been deliberately increased by making use of the

resonance technique. However, for studies of the temperature, field and orientation dependence of amplitude, only relative values of amplitude are required and the accuracy is considerably higher than that of the absolute values.

3. Orientation dependence of the periods

In order to have as large an amplitude as possible, all experiments on the orientation dependence of the periods were carried out at the lowest available temperature of 1·2 °K; no significant variation of period with temperature or field could be detected in the range 1·2 to 4·2 °K. Most of the results were obtained using specimens with a [100] axis along the wire and thus each plane of study contained the [100] symmetry direction. Check measurements were also made on crystals with [110] and [111] axes along the wires. The periods were measured at roughly 3° intervals in each plane and the results from some six planes were sufficient to enable the periods for any orientation to be obtained by interpolation.

The oscillations may be conveniently divided into three groups, α, β and γ as indicated in figure 2, which shows the variation of period with orientation in a (100) plane. Period values fall between $5{\cdot}4\times10^{-8}\,\mathrm{G}^{-1}$ for group γ at [110] and about $0{\cdot}53\times10^{-8}\,\mathrm{G}^{-1}$ for group α at [100]. Apart from oscillations of similar period in tin, the α-oscillations have the shortest period found so far in any metal. In regions where the amplitudes of the γ-oscillations have become unobservably small, the experimental curves have been produced as extrapolations (broken curves) in accordance with a scheme which will be explained in § 3 (*c*); no extrapolations were made for the β-oscillations. Because of the limitations of the rotating mechanism, experimental points were obtained only over a range of some 60° for any specimen and the remainder of figure 2 has been drawn so that the figure as a whole is symmetrical about [110]. We shall now discuss the nature of the oscillations in each of these groups in turn.

(*a*) *The α-oscillations*

On account of their short period, which implies large area of cross-section of the Fermi surface, the α-oscillations are perhaps of most interest. They have greatest amplitude in a [110] direction and usually appear superimposed on the slower γ-oscillations (figure 1*g* and *h*, plate 1). The period is practically the same for all orientations implying that the surface giving rise to the oscillations must be nearly spherical. Measurement of the period is difficult near [100] since the α-oscillations are swamped near this direction by the much stronger β ones, but the period appears to vary smoothly from about $0{\cdot}53\times10^{-8}\,\mathrm{G}^{-1}$ at [100] to about $0{\cdot}59\times10^{-8}\,\mathrm{G}^{-1}$ at [110]. This suggests that the surface may be drawn out from a sphere along [100] directions, though the observed variation is hardly larger than the uncertainty in period determination. If we treat the surface as a sphere corresponding to a mean period of $0{\cdot}56\times10^{-8}\,\mathrm{G}^{-1}$, its radius may be found from the diametral area of cross-section given by (1) and is $0{\cdot}57(2\pi/a)\,\mathrm{cm}^{-1}$ in **k**-space. Here $a = 4{\cdot}94$ Å is the lattice constant of the f.c.c. lattice, and the dimensions of the surfaces can best be compared with those of the Brillouin zone (§ 4) if the results are always expressed in this manner. The volume of the sphere is then $0{\cdot}80(2\pi/a)^3\,\mathrm{cm}^{-3}$ and, since the volume in **k**-space corresponding to 1 electron (or hole) per atom is $2(2\pi/a)^3\,\mathrm{cm}^{-3}$, we see that the sphere contains 0·40 electron or hole per atom.

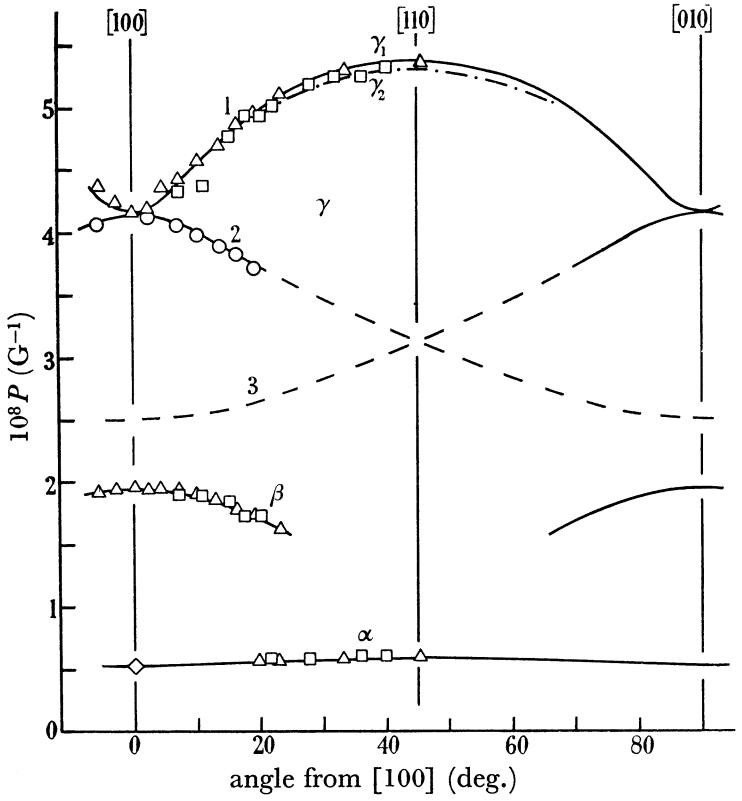

FIGURE 2

Notes relating to figures 2, 3 *and* 4. Each point in these figures is the mean of three or four separate period determinations. △, ▽, specimens with [100] axis along wire; □, specimen with [110] axis along wire; ◇, specimen prepared by 'strain-anneal' method; ○, calculated from beat period of 'short beats'; ——, extrapolation of group γ results in accordance with a scheme (γ_1) consisting of three branches 1, 2 and 3; ·—·—, additional term (γ_2) deduced from the 'long beats'. The points in branch 1 usually refer to the dominant of the two terms γ_1 and γ_2, but give the mean period near [110]. The period for group α is practically independent of orientation and the anisotropy of group β is the same in all planes containing a [100] axis; for these reasons groups α and β are not shown in figures 3 and 4. The behaviour of group α near [100] has been studied in more detail in a (110) plane, so that ◇ in figure 2 should not be regarded as an isolated point. The solid curves belonging to the three-period scheme of group γ are those obtained from a smoothed contour diagram of period which was prepared from the experimental points and which satisfied the requirements of cubic symmetry (see Gunnersen 1956); on account of small angular errors in the settings of the crystals, the solid curves thus drawn do not always appear to be the best curves through the experimental points. The points beyond 60° in figure 3 were obtained from the results in other planes, making use of cubic symmetry.

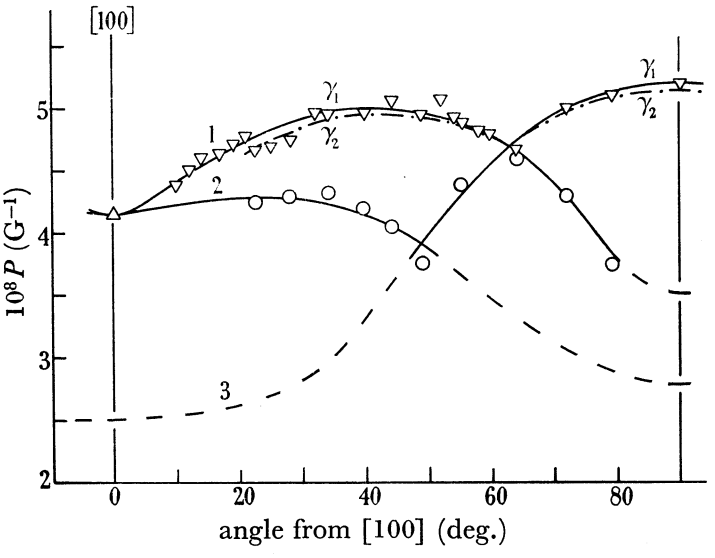

FIGURE 3

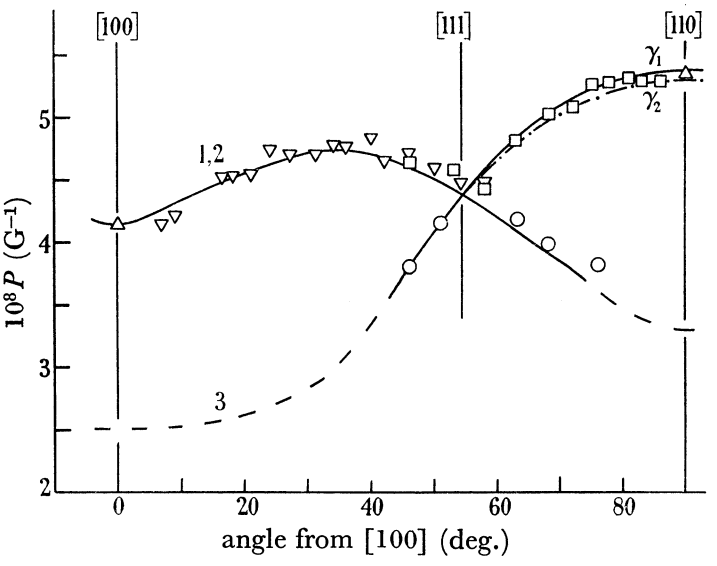

FIGURE 4

FIGURE 2. Variation of periods with orientation in a (100) plane, showing the division into three groups α, β and γ.

FIGURE 3. Variation of periods of group γ with orientation in a plane whose normal has direction cosines $\left(\frac{1}{2}\ \frac{\sqrt{3}}{2}\ 0\right)$.

FIGURE 4. Variation of periods of group γ with orientation in a (110) plane.

As may be seen from figure 1*h* (plate 1), complex modulations are often present in the α-oscillations. These are, however, always in phase with the slow γ-oscillations, suggesting that the modulations are due not to some multiplicity of surfaces, but rather to some intrinsic effect in the metal (such as a removal of electrons from one band into another in order to keep the Fermi level constant as the field is varied) or to some feature of the experimental method, which has not yet been understood. Subsidiary experiments suggested that the modulations were not associated with any lack of faithfulness in the amplification system.

(*b*) *The β-oscillations*

This group, which appears to consist only of a single term, has greatest amplitude in a [100] direction, where $P = 1{\cdot}94 \times 10^{-8}\,\mathrm{G}^{-1}$. The amplitude dies off extremely rapidly with orientation and the oscillations cannot be detected beyond an angle of about 25° from [100]. The anisotropy of period is found to be, within experimental error, the same as in figure 2 for all planes containing a [100] axis. Thus, the contributing part of the relevant surface appears to be a surface of revolution, and from the detailed variation of the period with orientation, it may be deduced that the surface consists of part of a hyperboloid of almost exactly zero eccentricity (rectangular hyperboloid). A discussion of how such a surface may arise will be deferred until § 4.

(*c*) *The γ-oscillations*

Group γ (experimental points between $P = 3{\cdot}7 \times 10^{-8}\,\mathrm{G}^{-1}$ and $P = 5{\cdot}4 \times 10^{-8}\,\mathrm{G}^{-1}$) is the most complex of the three groups. Examples of envelopes of these oscillations (figure 1 *a*, *b* and *c*, plate 1) shows beating patterns due in general to two and sometimes three terms of slightly differing period. The beats have 30 or more cycles per beat and so the constituent terms have periods differing by at most 3 %, this being of the same order as the scatter of the experimental points. In addition, shorter beats with as few as three or four cycles per beat can be observed in some orientations (figure 1*e*, plate 1); these represent much larger period differences. In attempting to fit these results into some scheme, the long beats were ignored as representing some 'fine-structure' effect (this is shown as a splitting of the longest period γ-oscillations into the two terms γ_1 and γ_2 in figures 2, 3 and 4 and will be discussed at the end of this section) and only the shorter beats were taken into account. The upper branch (labelled 1 in figure 2) is the dominant term and the points on branch 2 have been calculated from the short beats; it is not obvious from the points alone whether the experimental curves touch or cross at [100] although touching seems more likely. A third branch 3 has been drawn such that (in a (100) plane) branches 2 and 3 have twofold symmetry and are 'out-of-phase' with one another and reasons for doing so will be given shortly. Figure 3 shows the anisotropy of group γ in a plane whose normal has direction cosines $\left(\frac{1}{2}\,\frac{\sqrt{3}}{2}\,0\right)$ with respect to the tetrad axes; this plane contains a [100] axis and lies between (100) and (110) planes. It can be seen that branches 1 and 2 have now become much closer than in figure 2. In a (110) plane (figure 4), branches 1 and 2 have coalesced into a single curve and all three periods are equal in a [111] direction.

The three-period scheme that has been assumed in figures 2, 3 and 4, is of form similar to that found by Gunnersen (1956), working at fields of ~ 15 kG, for the fastest oscillations

in aluminium ($P \sim 2 \times 10^{-7}\,\mathrm{G}^{-1}$); the curves obtained in other planes (e.g. (111) and other planes intermediate between (100) and (110)) are of the same form as Gunnersen's and so have not been given here. In fact Gunnersen's period values for aluminium scale down almost exactly to those of lead, if reduced by a factor of 6·7. The experimental curves from the two metals then coincide exactly at [110] and [111], and the maximum misfit is about 6 % at [100]; this is, however, the orientation for which period measurement was least reliable in both experiments.

As in aluminium, the portions of Fermi surface which give rise to these oscillations can be made up of pieces containing electrons or holes and centred on either (i) the twenty-four corners W, or (ii) the centres X of the six square faces of the reduced Brillouin zone for the f.c.c. lattice (Gunnersen 1956, Heine 1957; see the lower half of figure 5). Both of these possibilities predict a three-period scheme due to three 'cushion-shaped' surfaces at right angles to one another. The three periods should have just the symmetry properties of the extrapolated curves drawn through the experimental points, with two of the branches coinciding in a (110) plane and all three periods equal in a [111] direction. In case (i) we have really six closed surfaces occurring in three pairs; one member of each pair is the inversion image of the other and so the pair gives rise to only one period for all orientations of magnetic field. In case (ii) there is no such doubling. Heine (1957) concluded that case (i) was appropriate for aluminium and that the surfaces contained holes, this being the only interpretation consistent with his detailed band-structure calculation. No such calculation has been attempted for lead, but we shall be able to conclude, from the discussion of § 4, that case (i) is again appropriate and that the surfaces contain electrons.

Since the periods in lead and aluminium are related by a scaling factor, we may use Gunnersen's calculation of the shape of the surfaces by the procedure of Lifshitz & Pogorelov (1954); this method gives a centro-symmetric surface whose central areas of cross-section are the same as the extreme areas of each member of the actual pair of surfaces (i.e. a kind of symmetrized hybrid). The six surfaces then account for a total of 0·11 electron per atom.

So far we have ignored the longest beats associated with the γ-oscillations. On the basis of the proposed three-period scheme, such long beats may be expected only in the branch 1, 2 in a (110) plane (figure 4); if, due to small angular errors, the plane of rotation is not exactly a (110) plane, the branch 1, 2 will split into two branches of slightly differing period. However, the long beats found at many other orientations find no simple explanation in terms of the three-period scheme. Since the period values appear to fall slightly at orientations where these beats commence (e.g. at 20° from [100] in figure 3), the periods of the additional terms giving rise to the beats are presumably shorter than those of the relevant branches of the three-period scheme. The period differences can be obtained from the beat periods and the additional terms are shown as the chain curves γ_2 in figures 2, 3 and 4; henceforth the branches associated with the three-period scheme alone will be referred to as γ_1. There is, furthermore, an increase in the overall amplitude of the relevant oscillations as soon as the long beats commence. These apparently puzzling results may be accounted for in a plausible manner in the light of the conclusions of § 4, where it will be shown that the additional terms γ_2 may, in fact, be associated with the β-oscillations.

PHILOSOPHICAL TRANSACTIONS OF THE ROYAL SOCIETY A MATHEMATICAL, PHYSICAL & ENGINEERING SCIENCES

4. The Fermi surface and the Brillouin zone scheme

(a) *The free-electron model*

In the absence of a theoretical band-structure calculation it was decided to use the simple free-electron model as a guide in fitting the observed surfaces into the Brillouin zone scheme, and it was hoped that even such a crude model might throw some light on the nature of the 'hyperboloidal' surface giving rise to the β-oscillations.

Lead will be assumed to have four valence electrons per atom and, if we ignore entirely the effect of the crystal lattice, these can be accommodated inside a sphere in **k**-space of volume

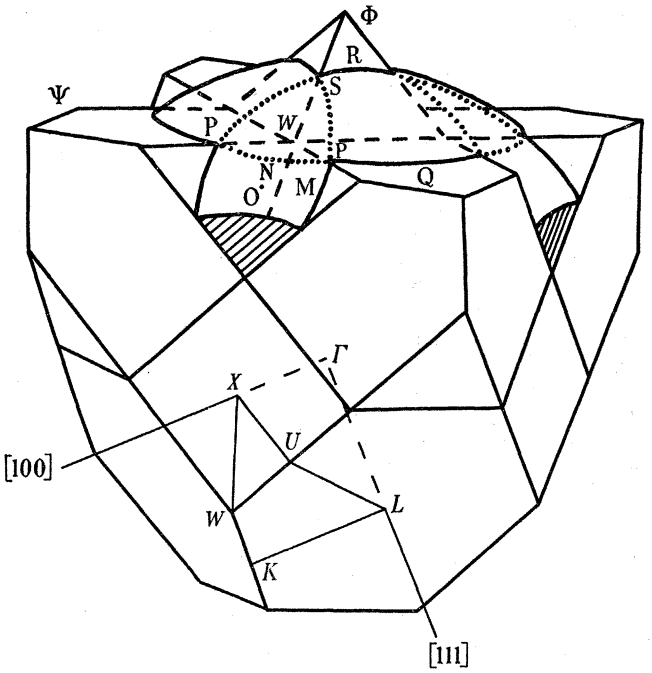

Figure 5

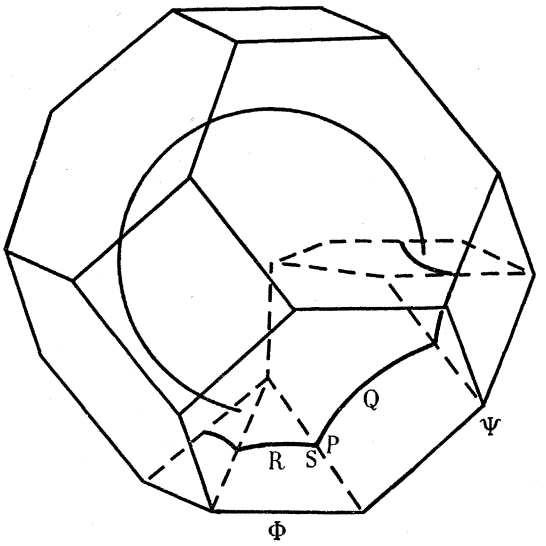

Figure 6

Figure 5. The free-electron model (extended zone scheme). Lower half: part of the first Brillouin zone; upper half: Φ, Ψ are portions of the second Brillouin zone and only that part of the free-electron sphere which lies without Φ, Ψ is shown. The italic capitals refer to specific points on the zone and the roman capitals refer to specific points on the free-electron sphere.

$$\Gamma X = 2WX = (2\pi/a)\ \mathrm{cm}^{-1} \quad \text{in} \quad \mathbf{k}\text{-space}.$$

Figure 6. The free-electron surface in the second zone. The letters correspond to letters equivalent to those in figure 5.

$8(2\pi/a)^3\,\mathrm{cm}^{-3}$, and hence radius $1{\cdot}24(2\pi/a)\ \mathrm{cm}^{-1}$. Figure 5 shows the relation of this sphere to the extended Brillouin zone scheme; part of the first zone (cell of the reciprocal lattice) is visible in the lower half of the diagram. The second zone is bounded by the same planes as the first (see, for example, Seitz (1940), p. 298) and consists of portions such as Φ and Ψ which fit over the square and hexagonal faces, respectively, of the first zone; to avoid confusion these are shown only in the upper half of the figure. The free-electron sphere completely surrounds the first zone and only part of the spherical surface which lies outside the portions Φ and Ψ has been shown. Most of this part of the surface belongs to the third zone, but the electrons within the spherical triangles bounded by the dotted lines (e.g.

*W*PSP) belong to the fourth zone. Thus, the first zone is filled with two electrons per atom and the remaining two electrons are distributed amongst the second, third and fourth zones.

Now it is always possible to remap the portions of each of the second and higher zones into a cell of the reciprocal lattice by translations of reciprocal lattice vectors. The result is the 'reduced zone scheme' and henceforth 'zone' will be taken to mean 'reduced zone'. This is illustrated for the second zone in figure 6, where one each of the portions Φ and Ψ' has been re-mapped in this manner. We see that the separate pieces of the free-electron surface within these portions now come together to form a single closed surface (as indicated by RSPQ) which will be somewhat indented. This closed surface, bounding an unfilled region of the second zone, may be regarded as containing holes. In reality there will be energy gaps across the planes of figure 5, distorting the original free-electron sphere, and we may suppose that the effect of these gaps is to smooth out the re-mapped second-zone surface and possibly to alter its size; a sphere of the same volume as the original indented surface is indicated in figure 6.

The portions containing electrons in the third and fourth zones in the extended zone scheme of figure 5 may likewise be re-mapped into the reduced zone scheme. The re-mapping is not quite so simple as for the second zone, since each of the portions must be broken up in a particular way and the pieces re-mapped separately. The result in the reduced third zone is a surface formed by electrons entering the zone along zone lines (illustrated schematically in the lower half of figure 7) and in the reduced fourth zone, pieces of surface are formed by electrons entering the zone at zone corners.

The numbers, as predicted by the free-electron model, of electrons or holes per atom in the various zones are of interest. An approximate calculation was made of the volume occupied by electrons in all the portions Φ, Ψ' of the second zone (figure 5); when this is subtracted from the volume of the zone we are left with the volume occupied by the holes (figure 6). The volume occupied in the third zone is not easily calculated directly and was obtained by finding first the total volume occupied by electrons in the fourth zone (i.e. twenty-four times that of *W*PSP in figure 5) and subtracting this from the volume occupied by the second-zone holes; for a metal of even valency, the volume of holes in an unfilled zone must be equal to the volume of electrons which spill over into higher zones. By dividing these volumes by $2(2\pi/a)^3\,\mathrm{cm}^{-3}$ we obtain 0·54 hole in the second zone, 0·48 electron in the third zone and 0·06 electron in the fourth zone.

(*b*) *Comparison with the experimental surfaces*

It is plausible to associate the almost spherical surface giving rise to the α-oscillations with the single closed free-electron surface in the second zone. The observed surface, whose volume (i.e. corresponding to 0·40 carrier per atom) is roughly three-quarters that of the free-electron surface, would thus contain holes. Furthermore, the cushion-shaped surfaces responsible for the γ_1-oscillations might be associated with the electrons which overlap into the fourth zone at zone corners. This then would correspond to case (i) of p. 93, with six closed surfaces containing electrons.

If the interpretation given so far is correct, it is evident that the 'hyperboloidal' surface must in some way be connected with the third-zone surface. We have seen that, on the free-

PHILOSOPHICAL TRANSACTIONS OF THE ROYAL SOCIETY A MATHEMATICAL, PHYSICAL & ENGINEERING SCIENCES

electron model, the third-zone surface is formed by electrons spilling over into the zone near zone lines (lower half of figure 7). The possibility of such complex surfaces giving rise to a de Haas–van Alphen effect may be best understood if, following Chambers (1956), we form a close-packed array of the reduced zones; one member of the array can be transformed into any other by translations of reciprocal lattice vectors. Three zones of the array meet along any line and the surfaces from each member link up to form a multiply connected surface of tubes extending throughout **k**-space. A portion of this surface, which can be

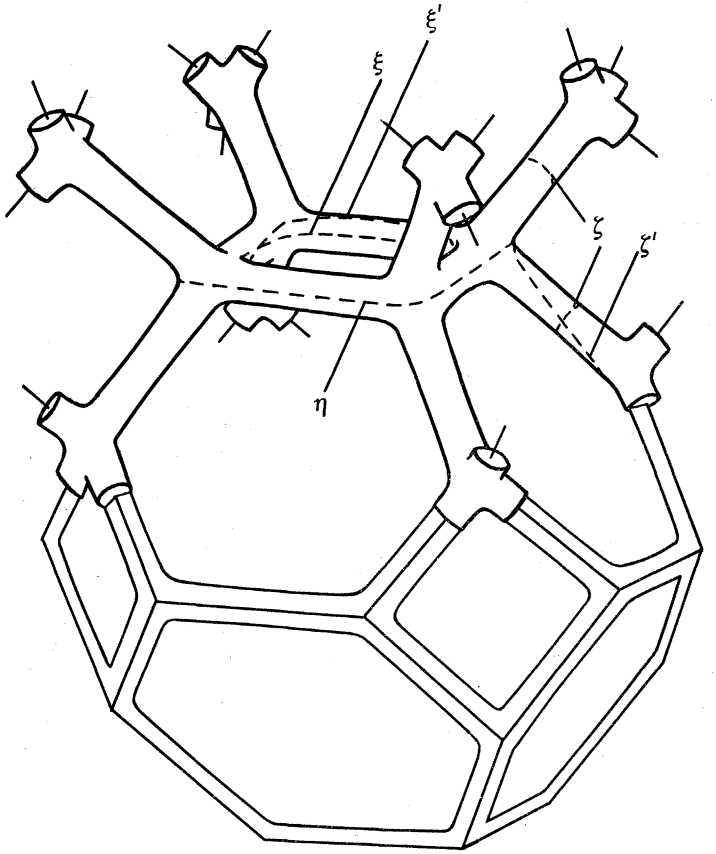

FIGURE 7. The free-electron surface in the third zone (schematic). Lower half: the surface in one cell of the reciprocal lattice; upper half: a portion of the multiply connected surface which is formed when the surface indicated in the lower half is repeated throughout the reciprocal lattice. For the sake of clarity the 'limbs' have been drawn considerably thinner than those of the actual free-electron surface and all sharp corners have been smoothed out. ξ, η and ζ are closed 'orbits' in **k**-space which might be expected to give rise to a de Haas–van Alphen effect.

regarded as consisting of zone lines 'thickened-up', is illustrated schematically in the upper half of figure 7. De Haas–van Alphen oscillations might then be expected from closed orbits of maximum or minimum cross-section in **k**-space, such as indicated by ξ, η and ζ.

Now the central section of the observed 'hyperboloid' (i.e. normal to a [100] direction) is of area $0{\cdot}30(2\pi/a)^2\,\mathrm{cm}^{-2}$, which fits comfortably into the area of a square face of the zone, $\frac{1}{2}(2\pi/a)^2\,\mathrm{cm}^{-2}$. Thus the β-oscillations may be plausibly accounted for by orbits of type ξ. We see also that the extreme area of cross-section should increase as the direction of the

field is moved away from [100], in agreement with the observed decrease in period, but the area cannot increase indefinitely. A critical angle will be reached beyond which an extreme area corresponding to type ξ orbits cannot be defined; this is illustrated by the limiting orbit ξ'. For this reason no extrapolation has been made of the β-oscillations in figure 2. The type ζ orbits should, according to the schematic surface drawn in figure 7, be of smallest area when the field direction is along a zone line ([110] direction) and such orbits can likewise be defined only over a limited angular range, as illustrated by the limiting orbit ζ'. Provided that the limiting angles from [110] (in all planes containing a [110] direction) are less than about 45°, it can be shown that the general form of the period anisotropy expected for oscillations arising from the type ζ orbits should have a character similar to that of the solid curves drawn through the experimental points of the γ-oscillations in figures 2, 3 and 4, except in the neighbourhood of a [100] direction. However, the angular ranges over which the oscillations should be observed will depend on the values of the limiting angles in various planes and these can be predicted only if the detailed shape of the surface is known. Thus oscillations arising from type ζ orbits provide a plausible explanation of the chain curves γ_2 in figures 2, 3 and 4. The fact that the chain curves come so close to the solid ones, so that the period values arising from the 'limbs' of the multiply connected surface in the third zone (i.e. γ_2) and the 'cushions' in the fourth zone (i.e. γ_1) are so nearly the same, may not be 'accidental'; a possible reason for this will be given on p. 102. No clear evidence has been found for oscillations arising from type η orbits.

(*c*) *Reliability of the interpretation*

The scheme proposed so far (summarized in the first two columns of table 1) appears to account satisfactorily in a qualitative way for all the observed groups of oscillations; however, the possibility that some alternative interpretation may be the correct one should not be overlooked.

We may first ask, in view of the remarks made in the preceding section, if the γ_1-oscillations as well as the γ_2-oscillations might not be due to the 'limbs' of the multiply connected third-zone surface, the fourth zone being completely empty. Such an interpretation might explain the absence of points in the broken curve regions of figures 2, 3 and 4 in terms of orbits ceasing beyond limiting angles, and so would get over the difficulty of explaining why the amplitudes of the shortest period oscillations in the three-period scheme should be unobservably small (the amplitudes will be discussed in detail in § 5). This disappearance of amplitude is a feature which was also found by Gunnersen (1956) for the corresponding oscillations in aluminium, but since he used the torque method, in which the amplitude is proportional to the rate of change of period with orientation, his lack of amplitude near [100] need not be very surprising; in the high-field method, however, there is no obvious reason why these oscillations should not show up. Tempting as the alternative interpretation is in being able to explain this feature, it is improbable for the following reasons. While the 'limbs' of the third-zone surface could account for most of the experimental points of the γ-oscillations, there is a discrepancy in the detailed behaviour near [100]. The alternative interpretation would require, for example, the crossing-over of two doubly degenerate curves at [100] in a (110) plane instead of a turning point in a single doubly degenerate curve as drawn in figure 4 (branch 1, 2). The presence of the two crossing curves should

manifest itself in beats of the γ-oscillations near [100] in this plane and no evidence for such beats has been found. Furthermore, the long beats in group γ could not be explained in such a simple manner if the above alternative interpretation were the correct one.

It has been tacitly assumed all along, that the beats in the γ-oscillations (they are strictly periodic in H^{-1} and their period and form are, for given crystallographic orientation, independent of the angle between the field and the specimen axis) are due to two or more extreme areas of the Fermi surface contributing simultaneously. This assumption would appear to be correct for the shorter beats, since the points deduced from the beat periods lie on smooth continuations of the curves drawn through the points obtained from direct period measurement (figures 3, 4). However, it is not out of the question that the remaining long beats, which have been attributed to the extra term γ_2 in figures 2, 3 and 4, might have some other explanation. For instance, beats might arise if, for experimental reasons, the oscillations are made up of several contributions of slightly differing period or phase. Thus, they might arise from the slight substructure which is known to be present in the crystals (see p. 106) or from an inhomogeneity of field within the specimen, caused by eddy currents; the substructure cannot, however, explain the long beats observed *at* [110] (figure 1*c*, plate 1), where the period has a stationary value, and eddy currents are unlikely to be of importance at such high fields (see p. 107).

Alternatively, the long beats might be due to some splitting or broadening of the magnetic energy levels. The possibility of a splitting arising from the coupling between the spin and the orbital motion of an electron can be rejected at once because of the inversion symmetry and the time-reversal symmetry of the one-electron wave function in a cubic metal (Kramers's theorem; see, for example, Elliott (1954)). Zilberman (1956, 1957) has shown that level broadening caused by the lattice potential may give rise to beating patterns, but for this to be so, either (i), the energy surfaces in neighbouring cells of the reciprocal lattice would have to be nearly in contact or (ii), there would have to be open-periodic orbits in **k**-space (Fermi surface an endless tube of variable cross-section, with the field normal to the axis of the tube). It is difficult to see how the general form of the period data could be interpreted in terms of (ii), but the possibility of broadening arising from (i) cannot be dismissed so readily. According to Zilberman (1956), the result of such a broadening, in its simplest form for nearly free electrons, is to modulate the amplitude of the oscillations by $J_0^2(\phi)$, where J_0 is the zero-order Bessel function and the argument ϕ is itself an oscillating function which varies with field as $aH^{-\frac{1}{2}}\sin(2\pi/bH-\frac{3}{4}\pi)$ (a and b are field independent quantities). Even if $J_0^2(\phi)$ is given its asymptotic form for large ϕ, namely, $J_0^2(\phi)\rightarrow 2\cos^2(\phi-\frac{1}{4}\pi)/\pi\phi$, it is difficult to see how this type of function can account for the observed strict periodicity in H^{-1} of the beats. However, the form of the broadening (and hence of any beating patterns produced) is very dependent on the nature of the assumptions made in such calculations so that we cannot reject with complete certainty the possibility of the long beats being due to this cause. From all these considerations, the interpretation given to the long beats in terms of the two components γ_1 and γ_2 seems the most likely one. (It should be mentioned that no explanation has been offered for the 'dip' at the middle of the long-beat pattern of figure 1*a* (plate 1) or for the form of the long beats in figure 1*b*; the long-beat patterns were generally found to be of a simple character as in figure 1*c*.)

Finally, it is improbable that all the surfaces associated with the observed oscillations can be fitted into the zone structure in any other manner than that proposed. If, for example, the cushion-shaped surfaces were made up of pieces containing holes at the corners of the first zone (as in aluminium), the second-zone surface could not be one of a single sheet and it would thus be difficult to account for an almost spherical surface of the size found. From considerations such as those presented in this section, the general form of the Fermi surface proposed appears to be the only one consistent with the facts.

(*d*) *Detailed shape of the Fermi surface*

Although application of the free-electron model has enabled the observed surfaces to be fitted into the Brillouin zone scheme in a consistent manner, the detailed shapes of the various parts of the Fermi surface would not be expected to agree with those of the free-electron surfaces because of finite energy gaps across the zone planes. We shall now make some more quantitative remarks concerning the third- and fourth-zone surfaces; the second-zone surface will be taken as spherical although it may in fact be extended a little in [100] directions.

It will be assumed that the section through the third-zone surface corresponding to the orbit ξ of figure 7 is more like a circle than a square; a (100) section through the surface is shown in figure 8*a*, in which ξ is taken as a circle of area $0{\cdot}30(2\pi/a)^2\,\mathrm{cm}^{-2}$ in accordance with the period data. By symmetry the distances $W\mathrm{N}'$ and $W\mathrm{N}''$ must be equal, but otherwise nothing is known about the orbit η. Although the area of the orbit ζ (i.e. the (110) section; figure 8*b*) is known from the period to be $0{\cdot}11(2\pi/a)^2\,\mathrm{cm}^{-2}$, we have no information about its shape. It must however pass through the point O′ which is fairly accurately known from orbit ξ, and two possible orbits are shown in figure 8*b*. For purposes of calculation we shall choose the circular one (the actual orbit does not require to meet the line LU normally (Bouckaert, Smoluchowski & Wigner 1936)). With this choice the point Q′, which lies on both η and ζ, is such that $X\mathrm{Q}' = 0{\cdot}65(2\pi/a)\,\mathrm{cm}^{-1}$; this is sufficiently close to $X\mathrm{N}'' = 0{\cdot}68(2\pi/a)\,\mathrm{cm}^{-1}$ to permit η to be considered circular also. Thus the surface may be considered approximately to consist of a series of 'anchor-rings' (tori), of radii $r_1 = 0{\cdot}50(2\pi/a)\,\mathrm{cm}^{-1}$ and $r_2 = 0{\cdot}19(2\pi/a)\,\mathrm{cm}^{-1}$ as shown, intersecting one another at right angles. The critical angle from [100], predicted by this model beyond which type ξ orbits cannot be defined, is 21°, in good qualitative agreement with the experimental values of between 20 and 25° for the end of the β-oscillations. In figure 8*a* and *b* the sections through the 'anchor-ring' model are compared with those through the free-electron surface and the actual surface is seen to be somewhat smaller than the free-electron one.

The volume per zone of the third-zone electrons is not just the volume of three separate 'anchor-rings', since each ring shares part of its volume with four others. Thus, from each ring we must subtract twice the volume which is common to two rings at an intersection. We have no information about the shape of the actual surface near such an intersection, but we may guess that the common volume can be taken roughly as the mean of that of a cube of side $2r_2$ and that of a sphere of diameter $2r_2$. The total volume per zone is then approximately $6\pi^2 r_2^2(r_1 - 0{\cdot}6r_2)$ (the second term represents the correction due to the common volume). This gives $0{\cdot}76(2\pi/a)^3\,\mathrm{cm}^{-3}$ and the surface thus contains 0·38 electron per atom. Similarly, when computing the total surface area, which will be required in the

subsequent discussion (§ 6 (*a*)), we must apply corrections because of the intersections. A reasonable estimate is to subtract twelve times the mean of the areas of a square of side $2r_2$ and a circle of diameter $2r_2$ from the area of each ring. The total area is then approximately $12\pi^2 r_2(r_1 - r_2)$, which gives $6{\cdot}9(2\pi/a)^2\,\mathrm{cm}^{-2}$.

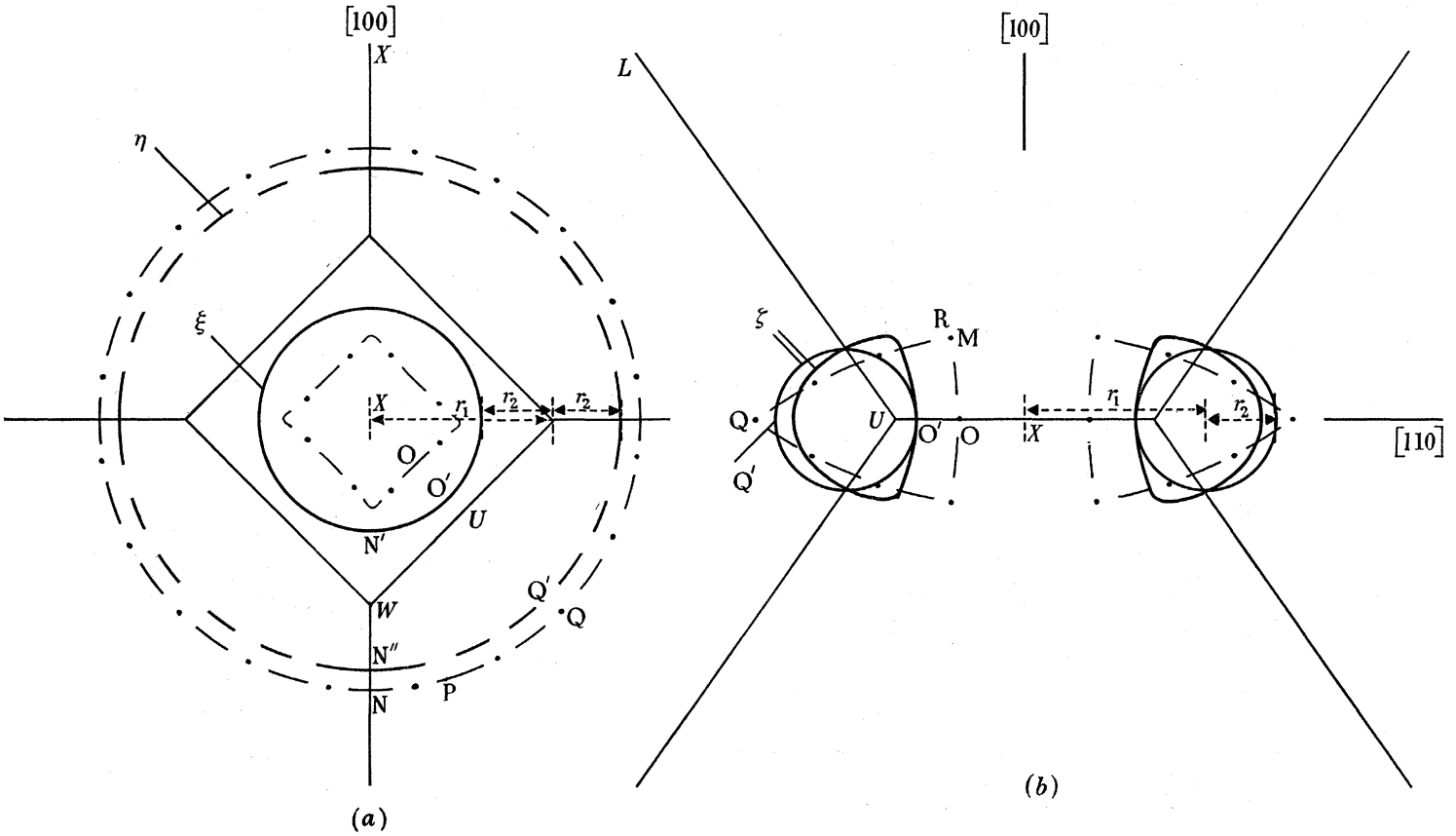

FIGURE 8. Details of the Fermi surface in the third zone. (*a*) (100) section; (*b*) (110) section; ——, sections through the proposed Fermi surface from which oscillations have been observed (two possible sections are shown in *b*); — —, section through the proposed Fermi surface from which oscillations have not been observed; · — · —, sections through the free-electron surface. ξ, η and ζ correspond to similar orbits in figure 7 and the unprimed capitals correspond to letters equivalent to those in figure 5. $r_1 = 0{\cdot}50(2\pi/a)$ cm^{-1} and $r_2 = 0{\cdot}19(2\pi/a)$ cm^{-1} are the principal radii of the 'intersecting anchor-ring' model for the third-zone surface.

We shall now compare the observed and the free-electron fourth-zone surfaces. Figure 9*a* and *b* shows two (100) sections through one of the fourth-zone surfaces, the third (100) section being the same as that in figure 9*a* but rotated through 90°. Each surface may be regarded as being made up of four of the pieces such as *W*PSP in figure 5 fitted together; how this is done may be better understood by comparing the lettering of figure 9 with that of figure 5. It will be seen that the shape of the symmetrized surface obtained by scaling up Gunnersen's (1956) results as explained in § 3 (*c*) ($\rho(a) = 0{\cdot}35(2\pi/a)\,\mathrm{cm}^{-1}$, $\rho(b) = 0{\cdot}23(2\pi/a)\,\mathrm{cm}^{-1}$ and $\rho(c) = 0{\cdot}14(2\pi/a)\,\mathrm{cm}^{-1}$) departs markedly from that of the free-electron surface. The actual surface will not be the same as the symmetrized one (although they must both have the same extreme areas of cross-section) and must meet the lines from *W* to P, S normally. We may, furthermore, set a limit to the size of the

actual surface by making use of our knowledge of the third-zone surface. In the extended zone scheme of figure 5, the distance WN to the free-electron surface (i.e. along a [100] direction) is, of course, the same whether measured just within the third zone or just within the fourth. This will no longer be true for the real surface since the

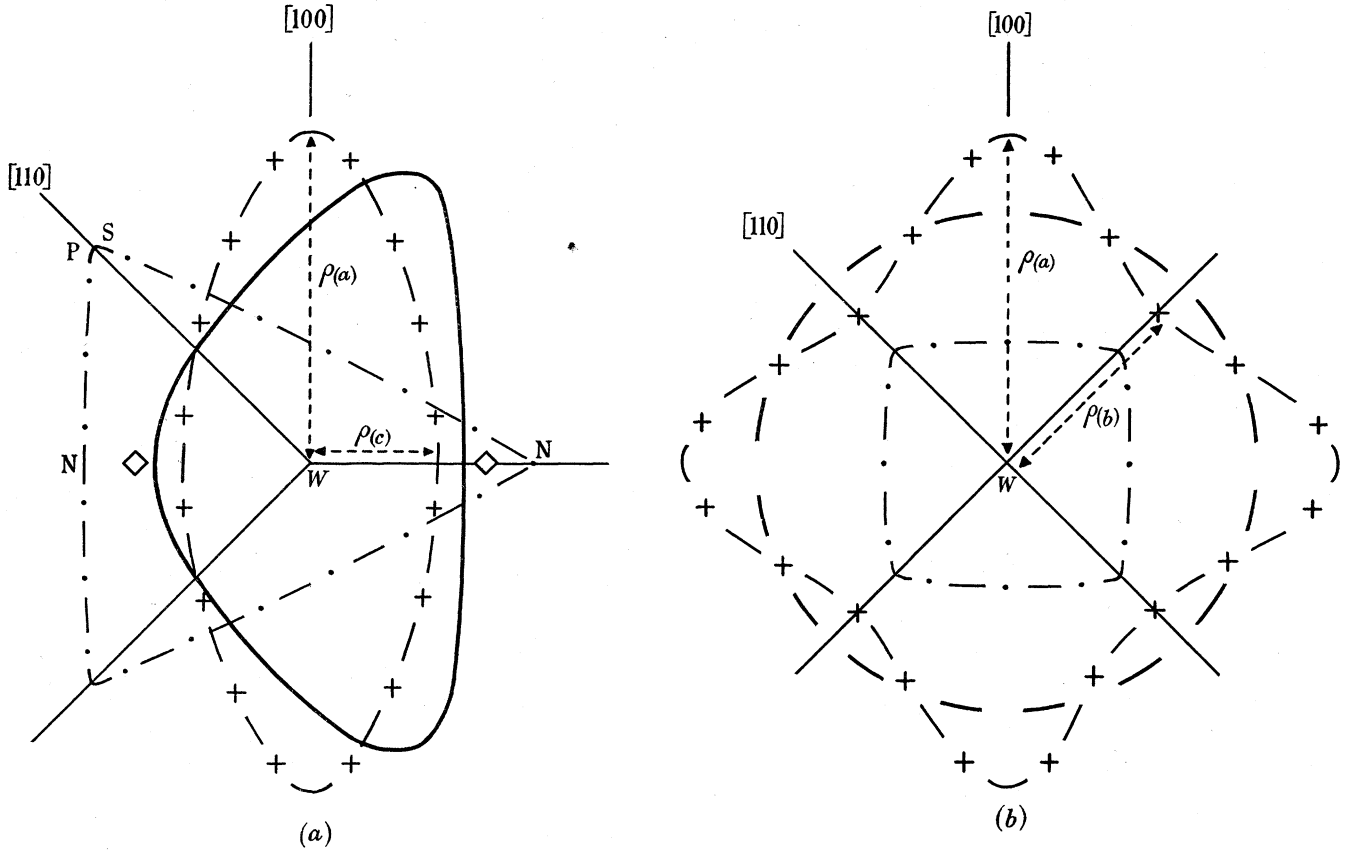

FIGURE 9. Details of the Fermi surface in the fourth zone. (a) and (b) are (100) sections; ——, probable section through the Fermi surface corresponding to $P = 4{\cdot}2 \times 10^{-8}\,\mathrm{G}^{-1}$ (section a); — —, probable section through the Fermi surface corresponding to $P \sim 2{\cdot}5 \times 10^{-8}\,\mathrm{G}^{-1}$ (section b; oscillations corresponding to this section have not been observed); +—+—, sections through one of the symmetrized 'cushion-shaped' surfaces; ·—·—, sections through the free-electron surface. The capitals correspond to letters equivalent to those in figure 5. $\rho(a) = 0{\cdot}35(2\pi/a)$ cm^{-1}, $\rho(b) = 0{\cdot}23(2\pi/a)$ cm^{-1} and $\rho(c) = 0{\cdot}14(2\pi/a)$ cm^{-1} are dimensions of the symmetrized surface. The points ◇ are limits to the size of the actual surface which have been inferred from knowledge of the third-zone surface.

free-electron energy surfaces will be modified by the presence of the energy gap between the third and fourth zones, and the distance WN′ to the actual surface in the third zone must always be greater than the corresponding distance in the fourth zone. Now WN′ is known fairly accurately from orbit ξ of figure 8a and this means that the fourth-zone surface must not extend beyond the points ◇ in figure 9a. One of many possible surfaces drawn with these restrictions is shown; it is found necessary to draw it fairly close to the limiting points ◇ from which we conclude that the energy gap between the third and fourth zones near zone corners must be very small. In other words, if the third- and fourth-zone surfaces are re-mapped back into the extended zone scheme, they should very nearly merge smoothly

into one another, with only small discontinuities where they cross zone planes. It is, in fact, because of the smallness of the energy gap that we have the near coincidence of the periods of the γ_2- and γ_1-oscillations from the third- and fourth-zone surfaces, respectively.

A possible reason for the smallness of the gap has been suggested by Heine (private communication). According to the free-electron approximation, there are four degenerate states (excluding spin degeneracy) at the zone corners. In a periodic potential, however,

TABLE 1. PROPOSED FERMI SURFACE IN LEAD

zone	nature of surface(s)	total carriers per atom within surface(s)	total surface area in **k**-space $\times 10^{-16}$ (cm^{-2})	$10^{-8}\bar{v}_0$ (cm s^{-1})	$10^{-3}\gamma$ (electronic specific heat) (erg cm^{-3} deg.$^{-2}$)
1	zone full	[2·00 (2·00) electrons]	—	—	—
2	sphere at centre of zone	0·40 ± 0·05 (0·54) hole	6·6 ± 0·5	0·84 ± 0·15 (1·83)	0·38 ± 0·06
3	multiply connected surface round zone lines	0·38 ± 0·15 (0·48) electron	12·0 ± 4·0	0·33 ± 0·06 (1·83)	1·73 ± 0·60
4	six 'cushion-shaped' surfaces from pieces at zone corners	0·11 ± 0·06 (0·06) electron	6·9 ± 1·5	0·35 ± 0·15 (1·83)	0·59 ± 0·25
5	zone empty	—	—	—	—
	totals from all zones		25·5 ± 4·3	—	2·70 ± 0·65
	free-electron values		(31·6)	—	(0·83)

Notes

(1) The free-electron values are given in round brackets.

(2) It is difficult to assess the accuracies of the various entries in view of the many approximations made. The results quoted for the second zone are the most reliable, since the surface approximates very closely to a sphere and the probable errors of the volume and surface area are based on the estimated probable error of P. For the third- and fourth-zone surfaces we can only guess how reliable the simplified models are. For example, the correction term in the estimation of the volume of the third-zone surface is probably only reliable to 30 %; since this term amounts to about 25 % of the total volume, the resulting error in the total volume should not exceed 10 %. If we suppose that the probable errors in the relevant periods and in the reliability of the 'anchor-ring' model may be expressed as 10 % inaccuracies in the radii r_1, r_2 of an 'anchor-ring', this suggests that a probable error for the total volume is 40 %. In estimating the fourth-zone volumes we have replaced the actual surfaces by the symmetrized 'cushions', whose volumes are estimated from approximate models, and we can only guess that the uncertainty involved is of the same order as that for the third-zone surface. Furthermore, the volumes of the 'cushions' depend on the extrapolated value of the period at [100] in branch 3 of the γ-oscillations and this may be reliable to only 30 %. Thus it is doubtful if the accuracy of the volume of the fourth-zone surfaces is better than about 60 %. The uncertainties quoted for the values in the last two columns of the table (§ 6(*a*)) take into account the probable errors in the surface sizes and in the values of m^*.

these four states are split up into two singlet states and two degenerate ones (Bouckaert *et al.* 1936). The fact that the actual band structure bears fair resemblance to the free-electron model suggests that it might be a good approximation to represent the wave functions by simple orthogonalized plane waves. If this is so, then the fact that lead is a heavy atom leads one to expect that the doubly degenerate state applies to the third and fourth zones and this would give a natural explanation for the small energy gap between these zones near zone corners.

The volumes and surface areas of the fourth-zone surfaces have been estimated from models which approximate to the symmetrized 'cushions'. Treating the section of figure 9*b*

as a square of side $2\rho(b)$ and assuming that all sections normal to the vectors $\rho(b)$ are ellipses, the volume per 'cushion' turns out to be $\pi^2\rho(b)^2\rho(c)/2$. This gives for the six 'cushions' $0{\cdot}22(2\pi/a)^3\,\mathrm{cm}^{-3}$ corresponding to a total of 0·11 electron per atom (as already quoted on p. 93). The surface area per 'cushion' was taken to be the mean of twice the total area of the slant faces of a pyramid of side $2\rho(b)$ and apex height $\rho(c)$. (i.e. $8\rho(b)\,(\rho(b)^2+\rho(c)^2)^{\frac{1}{2}}$), and the surface area of a rectangular box with square base of side $2\rho(b)$ and height $2\rho(c)$ (i.e. $8\rho(b)\,(\rho(b)+2\rho(c))$). Multiplying the mean by six, this gives $4{\cdot}3(2\pi/\mathrm{a})^2\,\mathrm{cm}^{-2}$ as the total area of the fourth-zone 'cushions'.

The conclusions of this paragraph are summarized in table 1 (the last two columns of the table will be discussed later). A first check on the correctness of our interpretation comes from the total number of electrons per atom. If we obtain the number of electrons in the second zone by subtracting the number of holes from 2·00, and add together the numbers of electrons in all zones, we arrive at $4{\cdot}09\pm0{\cdot}17$ per atom; this agrees satisfactorily with ascribing 4 valence electrons to lead. We also see that the total area of the Fermi surface is about two-thirds of that of the free-electron sphere containing 4 electrons per atom. Comparisons with other experimental evidence will be given in § 6 (*a*).

5. Further information from the de Haas–van Alphen effect

(*a*) *Temperature and field dependence of amplitude*

The theoretical amplitude of the oscillations in differential susceptibility $\mathrm{d}I/\mathrm{d}H$ may be obtained from the final expression given by Lifshitz & Kosevich (1955) and is

$$A=\left|\frac{\mathrm{d}I}{\mathrm{d}H}\right|\doteq\frac{16\pi^2kT}{h^3P^2H^{\frac{1}{2}}}\left(\frac{eh}{c}\right)^{\frac{3}{2}}\left|\frac{\partial^2\mathscr{A}}{\partial\mathbf{k}_H^2}\right|_0^{-\frac{1}{2}}\exp\left\{\frac{-4\pi^3m^*k(T+x)\mathrm{c}}{ehH}\right\}\cos\left(\pi\frac{m^*}{m_0}\right),\qquad(3)$$

where I is the magnetic moment per unit volume, k is the Boltzmann constant, m^* is the 'effective mass' defined by (2) and $|\partial^2\mathscr{A}/\partial\mathbf{k}_H^2|_0$ is a factor depending on the variation with wave vector of the area of cross-section of the Fermi surface normal to the field in the neighbourhood of the extreme area $\mathscr{A}_0$; it is a dimensionless quantity and has value 2π for a spherical surface. The cosine term, which gives an estimate of the reduction in amplitude due to electron spin, was derived by Dingle (1952*a*), who also showed (Dingle 1952*b*) that the effect of broadening due to collisions could, on various assumptions, be represented by a factor $\exp(-2\pi m^*c/\tau eH)$, where τ is the mean collision time. Writing $x=h/2\pi^2k\tau$, we see that this is equivalent to replacing the temperature in the exponent of (3) by an 'effective temperature' $T+x$. The approximate equation (3) is valid provided that $PH\ll1$ and harmonic terms need not be included if the numerical value of the exponent is appreciably greater than unity. Both these conditions are satisfied for the oscillations in lead.

The 'effective mass' m^* may be obtained from the temperature dependence of amplitude. According to (3), a plot of $\ln(A/T)$ against T (at some fixed value of H) should yield a straight line of slope $-4\pi^3m^*kc/ehH$. The amplitudes of the various oscillations were measured at various temperatures between 1·2 and 4·2 °K and good straight lines obtained. Figure 10 shows values of m^*/m_0 for various orientations in a (100) plane. It should be mentioned that the two terms γ_2 and γ_1 (which we have associated with orbits ζ of the third-zone surface

PHILOSOPHICAL TRANSACTIONS OF THE ROYAL SOCIETY A MATHEMATICAL, PHYSICAL & ENGINEERING SCIENCES

and orbits from the fourth-zone 'cushions') not only have similar period but also similar 'effective mass'. Thus the ratio of their amplitudes was independent of T to within about 10% in the range 1·2 to 4·2 °K. The 'effective mass' data will be used in § 6 (*a*) to make an estimate of the electronic specific heat.

Similarly, if ln $(AH^{\frac{1}{2}})$ is plotted against H^{-1} we should again have a straight line, of slope $-4\pi^3 m^* k(T+x)\, c/eh$. Thus knowing m^* from the temperature dependence, we can estimate the 'broadening temperature' x from the field dependence. The points did in fact lie on straight lines, but with rather more scatter than for the temperature dependence. Mean values of x were 1·3 °K for group β at [100] and 2·0 °K for group γ at [110]. Values

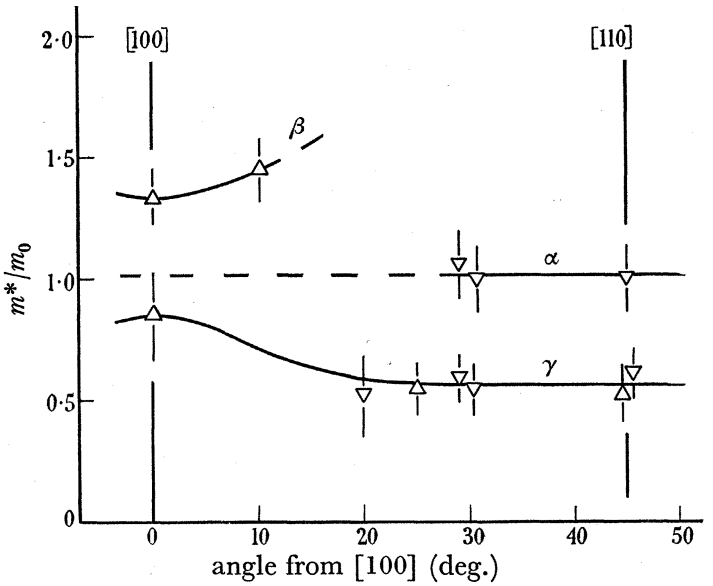

FIGURE 10. Variation of 'effective mass' for the α-, β- and dominant γ-oscillations with orientation in a (100) plane. The different sets of points are for two different specimens.

for group γ decreased to about 1·3 °K for orientations roughly midway between [100] and [110] in a (100) plane; this can be seen qualitatively from the relatively large amplitude at low fields in figure 1 *a*, when it is compared with figure 1 *c* (plate 1). The α-oscillations could not be observed over a sufficient range of fields to make a determination of x possible. The values of x did not appear to vary with temperature and were, for given crystallographic orientation, independent of the angle between the field and the specimen axis. Taking $x = 1{\cdot}5$ °K as representative of the results, this is equivalent to a collision time τ of $1{\cdot}6 \times 10^{-12}$ s. From measurements of the low-temperature resistance of several actual specimens (superconductivity was destroyed by application of a 'longitudinal' magnetic field and the results were extrapolated to zero field), the resistivity at 1·2 °K was found to be $1{\cdot}5 \times 10^{-4}$ times that of the room-temperature value. Assuming one carrier of normal mass per atom, the resistivity collision time τ_R at room temperature may be estimated as about $0{\cdot}5 \times 10^{-14}$ s and this then gives τ_R at 1·2 °K as 35×10^{-12} s. Though this estimate is very rough, it is clear that it would lead to a much smaller broadening of the de Haas–van Alphen levels than that suggested by the field dependence data. Similar results have been found in other pure metals at low fields (see, for example, Shoenberg 1952) and no convincing explanation has yet been found.

(b) Orientation dependence of amplitude and comparison with theory

The orientation dependence of the amplitude in a (100) plane is shown somewhat schematically in figure 11. The amplitude of the dominant γ-oscillations has been split into the two components γ_1 and γ_2 and, because of its abrupt rise at $\sim 25°$ from [100], we associate the higher amplitude with the γ_2 term (type ζ orbits of the third-zone surface). Since P, m^* and x are now known, it should be possible to compare these observed amplitudes with

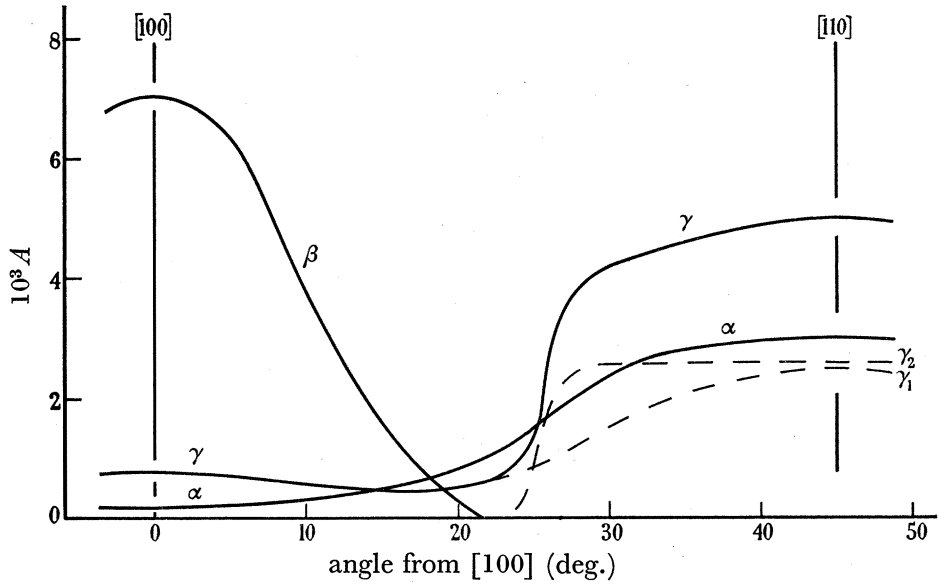

FIGURE 11. Variation of amplitude of the α-, β- and dominant γ-oscillations with orientation in a (100) plane (schematic). $T = 1{\cdot}2\,°\mathrm{K}$; $H = 70$ kG for group α and 60 kG for groups β and γ. The total amplitude of the γ-oscillations beyond $\sim 25°$ from [100] is the sum of the amplitudes of the two terms γ_1 and γ_2.

TABLE 2. COMPARISON WITH THEORETICAL AMPLITUDE AT $T = 1{\cdot}2\,°\mathrm{K}$

oscillations	H (kG)	x (°K)	m^*/m_0	exponent in (3)	$\lvert\cos(\pi m^*/m_0)\rvert$	$10^5 A_{\mathrm{calc.}}$	$10^5 A_{\mathrm{obs.}}$
α at [110] (second-zone surface)	70	(1·34)	1·0 ±0·1	(5·34)	0·96 to 1·0	(300)	300
β at [100] (orbit ξ of third-zone surface)	60	1·3 ± 0·3	1·33 ± 0·15	8·2 ± 1·4	0·2 to 0·8	0·1 to 4·0	700
γ_2 at [110] (orbit ζ of third-zone surface)	60	2·0 ± 0·5	0·56 ± 0·06	4·4 ± 0·9	0 to 0·3	0 to 10	250
γ_1 at [110] (dominant from fourth-zone surfaces)	60	2·0 ± 0·5	0·56 ± 0·06	4·4 ± 0·9	0 to 0·3	0 to 10	250

those predicted by (3). In doing this it must be remembered that, while the α- and β-oscillations each arise from only one orbit round the appropriate portions of Fermi surface, *each* of the two components γ_1 and γ_2 is due to two periods which are identical for all directions of field, i.e. the values obtained from (3) must be doubled in these cases. For lack of information about the detailed geometry of the surfaces, the factor $\lvert \partial^2 \mathscr{A}/\partial \mathbf{k}_H^2 \rvert_0$ has been taken as 2π, the value for a sphere. The comparison is given in table 2 for the orientations

at which the amplitudes are greatest, and estimates have been made of the reliability of the values predicted by (3) from the uncertainties in P, m^* and x.

The value of x for the α-oscillations could not be determined directly, but the amplitude predicted by (3) for these oscillations can be made to agree with the observed amplitude by choosing $x = 1{\cdot}34\,^{\circ}\mathrm{K}$. This choice seems reasonable since it is of the same order of magnitude as the value of x found for the other groups. However, the observed amplitudes of the β- and dominant γ-oscillations are much greater than the predicted ones. Part of this increase might be accounted for by supposing that the surfaces do not have 'spherical curvature' at these orientations. In the case of the β-oscillations, for example, the 'hyperboloidal' part of the third-zone surface may have a central region rather like a cylinder so that the orbit ζ in figure 8*b* may in fact resemble the non-circular one; however, this is unlikely to account for such a large discrepancy. We shall see below that there are several experimental features which can reduce the predicted amplitude, but it is difficult to think of an experimental feature whereby the amplitude might be increased. Possibly the discrepancy lies in some inapplicability of the theoretical formula (3) to such complex surfaces.

It is difficult to deduce the orientation dependence of amplitude from (3) in order to make a comparison with the experimental results in figure 11. For although the angular variations of P and m^* are known we really know nothing about the variations of the factors $|\partial^2\mathscr{A}/\partial\mathbf{k}_H^2|$ and x. Assuming, for all orientations, that $|\partial^2\mathscr{A}/\partial\mathbf{k}_H^2| = 2\pi$ and that x may be given the values quoted in table 2, equation (3) predicts angular variations of the amplitudes which are much smaller than the marked variations observed. This need not be too suprising since theory and experiment do not agree as far as the maximum amplitude of the β- and γ-oscillations are concerned.

A factor which may reduce the amplitude whenever the period varies rapidly with orientation is the presence of a substructure within the specimens; the reduction should be greatest for short periods and should be negligible at orientations where the period has a maximum or minimum value. To see if this was of importance for lead, Laue photographs were taken of the specimens using a micro-focus technique. These showed that the crystals appear to consist of a bunch of 'rods' parallel to the wire axis (cellular growth; see Martius (1954), Tiller (1957)). While the geometrical axis of each rod appears to be of the same crystallographic direction, the crystal axes normal to the rods appear to be misoriented relative to one another by rotations of the crystal axes about the geometrical axis. The mean misorientation is found to be as much as $\frac{1}{2}^{\circ}$ and such an angular spread could well account for most of the variation of the amplitudes of the β- and dominant γ-oscillations in between orientations where the period has a turning value, but clearly cannot explain the relatively low amplitudes of the α- and dominant γ-oscillations *at* [100]. In order to try to reduce the angular spread, a specimen was grown by the 'strain-anneal' method (though this was not found easy). Unfortunately, the Laue spots for the 'strain-anneal' specimen were found to be almost as broad as in the normal specimens, but the broadening was more uniform and did not indicate a 'rod-like' substructure. It was found in this specimen that the amplitudes of the α-oscillations near [100] were enhanced, though there was no appreciable difference in the other groups. Thus, while we have not been able to prove this with certainty, it is likely that crystal imperfection is one of the main factors controlling the variation of amplitude with orientation. It was also found that the

amplitudes for any particular orientation could be increased by a factor of two or so by growing the crystals so that this orientation coincided with the geometrical axis of figure. This was observed even at orientations where the period was a maximum or minimum (i.e. where substructure should be irrelevant) and no explanation has been found for this observation.

Since the field varies with time, eddy currents are induced in the specimen and cause an inhomogeneity of field, which could again reduce the amplitude. Because of the high magneto resistance of lead, this effect is not in practice important. Calculation shows that, for the field along the wire and for the particular field pulse and specimen size used in these experiments, the effect of eddy currents should become serious only at fields below 55, 45 and 35 kG for the α-, β- and dominant γ-oscillations, respectively; the amplitudes discussed above were measured at higher fields.

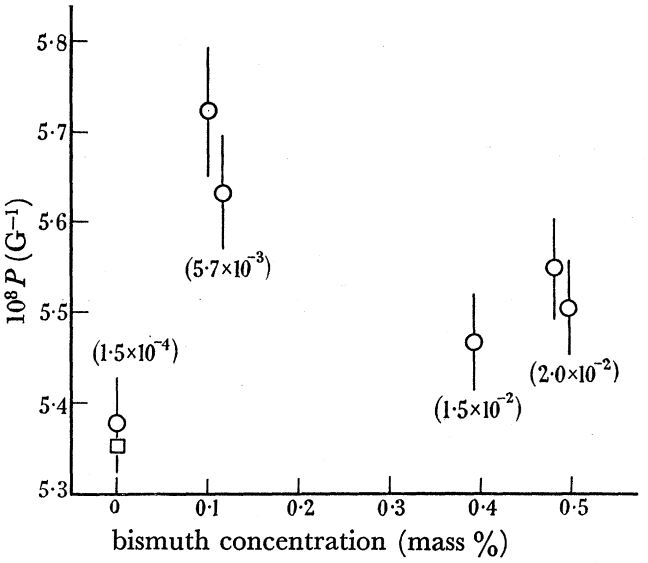

FIGURE 12. Variation of period of the dominant γ-oscillations (at [110]) with bismuth concentration in dilute lead-bismuth alloys. □ period from orientation-dependence studies in pure lead (figures 2 and 4). The numbers given in brackets are measured values of the ratio of the resistance at 1·2 °K to that at room temperature.

In contrast to the very large maximum amplitudes of the β- and γ-oscillations, the amplitudes of group γ become unobservably small when P falls below about $3{\cdot}7 \times 10^{-8}\,\mathrm{G}^{-1}$ (broken curve region in figures 2, 3 and 4; this feature has already been mentioned in § 4 (*c*)). The reduction in amplitude expected from the substructure in the crystals (together with an assumed increase in m^*) might partly account for this lack of results, but cannot explain the vanishingly small amplitude of branch 3 at [100] where the period should have a turning value.

(*c*) *Period and amplitude in dilute lead-bismuth alloys*

In order to decide experimentally whether electrons or holes are responsible for the various oscillations, an attempt was made to detect a change in period when lead was alloyed with small quantities of bismuth. A substitutional solution of bismuth in lead may be obtained with up to 15 % bismuth concentration (Solomon & Morris-Jones 1931; Meissner, Franz & Westerhoff 1932). Ingots of the alloys were annealed *in vacuo* at 300 °C for 18 days before

extrusion, and the single crystal wires (grown from seed as before) were annealed *in vacuo* for 30 days at 300 °C in the hope that this would reduce the inhomogeneities caused by the crystallization process. The dominant γ-oscillations at [110] could be detected, using the resonance technique, in specimens with up to 0·5 % bismuth but the amplitudes of the α- and β-oscillations became vanishingly small with as little as 0·13 % bismuth. After the experiments it was verified that the residual resistance of the actual specimens increased linearly with nominal bismuth concentration. The group γ period values for the alloys were all found to lie above that for pure lead (figure 12). This suggests that the relevant surfaces contain holes rather than electrons, thus apparently contradicting the proposed model. However, the increase is by no means monotonic and it is possible that the interpretation of the period shift may be more complicated than that expected from a simple 'rigid-band' model (Heine 1956).

The amplitude decreased more or less exponentially with increasing bismuth content showing by (3) that the *increase* in level broadening in the alloys could be ascribed to ordinary collisions. From the amplitude data it was possible to estimate the room-temperature collision time (in the same way as was done by Shoenberg (1952) for tin) to be $1{\cdot}6\times10^{-14}$ s, which is in reasonable agreement with the rough estimate of $0{\cdot}5\times10^{-14}$ s from the resistivity (see p. 104).

6. Discussion

(*a*) *Comparison with other experimental evidence*

From measurements of the anomalous skin resistance in polycrystalline lead, Chambers (1952) deduced that the total area of the Fermi surface was 0·46 times that of a sphere containing 4 electrons per atom, i.e. the area in **k**-space is $14{\cdot}5\times10^{16}\,\mathrm{cm}^{-2}$. Since the specimen used by Chambers had a poor surface polish, the true value may be up to 50 % greater (see appendix to Faber & Pippard 1955; the total surface area is proportional to the cube of the conductivity in the extreme anomalous limit), and may therefore be considered as in reasonable agreement with the estimate of $25{\cdot}5\times10^{16}\,\mathrm{cm}^{-2}$ given in table 1. Further confirmation of the proposed Fermi surface, as regards the total number of electrons and holes per atom, comes from studies of low-temperature galvanomagnetic effects (in polycrystalline lead) by Borovik (1954). Borovik analyzed the data in terms of a simple spherical two-band model and finds 0·5 electron and 0·5 hole per atom, again in reasonable agreement with the estimates in table 1.

The coefficient γ in the electronic term of the low-temperature specific heat is proportional to the density of states at the Fermi surface and may be estimated on the basis of the proposed model under certain simplifying assumptions. Thus, if the shapes of the surfaces are known, and also the manner in which the extreme areas of cross-section vary with energy (from the 'effective masses'), the volume between neighbouring energy surfaces, and hence the density of states, can be found. Alternatively, it may be more convenient to obtain the density from the integral of the reciprocal of the Fermi velocity over the surface. The formulae for γ (in erg $\mathrm{cm}^{-3}\,\mathrm{deg.}^{-2}$) are

$$\gamma = (k^2/12\pi)\,(\partial V/\partial E)_0, \tag{4a}$$

or

$$\gamma = (k^2/6h)\int \mathrm{d}S/v_0 = (k^2/6h)\,S/\bar{v}_0, \tag{4b}$$

where the volume V and area S are in $\mathbf{k}$-space, $\bar{v}_0$ is an appropriate average of Fermi velocity defined by (4*b*) and k is the Boltzmann constant.

For the second- and fourth-zone surfaces, γ was estimated from the volume between neighbouring energy surfaces. In the case of the second-zone surface, it was assumed that these were concentric spheres and that $m^* = m_0$; this does not necessarily imply quadratic dependence of energy on wave vector. It was assumed that the fourth-zone surfaces could be represented by the approximate form of the symmetrized 'cushions' used in estimating their volume (§ 4 (*d*)) and also that neighbouring surfaces were of the same shape. On these assumptions it is necessary to know the 'effective mass' for only one orientation; m^* was taken as $0{\cdot}56m_0$ in a [110] direction. For the multiply connected surface it was assumed that the orbits corresponding to ξ and ζ (figure 8) on neighbouring energy surfaces could be taken as concentric circles. For orbit ξ this should be fairly reasonable, but not necessarily so for orbit ζ (the lowest energy in the section of figure 8*b* is at U, not at the centre of the circle). However, the average velocities round these two orbits (from the period and

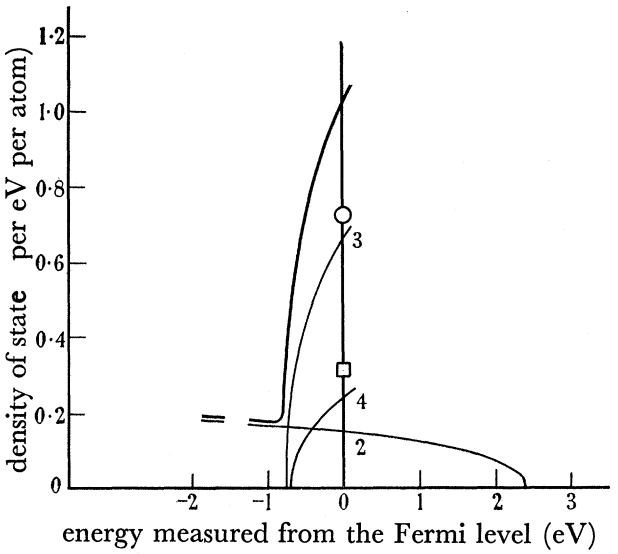

FIGURE 13. Curve of total density of states *against* energy, near the Fermi level (schematic). The contributions from the second-, third- and fourth-zone surfaces are also shown. The densities of states at the Fermi level (per eV per atom) are obtained by multiplying the γ values (in erg cm^{-3} deg^{-2}; table 1) by the factor $1{\cdot}60 \times 10^{-12}(3/2\pi^2k^2)\ (a^3/4) = 0{\cdot}38 \times 10^{-3}$ and the total at the Fermi level is reliable to about 25%. ○, experiments of Dolecek (1954); □, free-electron model (the free-electron Fermi energy is 9·5 eV).

'effective mass' values) do not differ much; they are $0{\cdot}35 \times 10^8$ cm s^{-1} and $0{\cdot}31 \times 10^8$ cm s^{-1}, respectively, so that a mean of $0{\cdot}33 \times 10^8$ cm s^{-1} should be a fair approximation to $\bar{v}_0$. The contribution of this surface to the specific heat was obtained by dividing this value into the surface area.

The results of these estimates and average values of the Fermi velocity are given in table 1. The velocities for the second- and fourth-zone surfaces were obtained from the densities of states and the areas of the surfaces. In view of the many approximations made here, the value of $2{\cdot}7 \times 10^3$ erg cm^{-3} deg.$^{-2}$ for the total γ from all parts of the Fermi surface may be considered to agree reasonably well with the value of $1{\cdot}88 \times 10^3$ erg cm^{-3} deg.$^{-2}$ obtained

by Dolecek (1954) from studies of the latent heat at the transition to superconductivity (see also appendix to Faber & Pippard 1955).

We shall now indicate what the density of states *against* energy curve must look like near the Fermi level. For quadratic dependence of the energy E on $\mathbf{k}$ (ellipsoidal energy surfaces), (1) reduces to

$$P = (e\hbar)/m^* c E_0', \tag{5}$$

where E_0' is the energy at the Fermi surface measured from the point of lowest or highest energy in the zone (depending on whether we are considering surfaces containing electrons or holes). Literal application of (5) gives $E_0' = 2\,\text{eV}$ for the second-zone sphere and $E_0' = 0{\cdot}4\,\text{eV}$ for both the 'limbs' of the multiply connected surface and the 'cushions'. The 'limbs' and 'cushions' are certainly not ellipsoidal, but 0·4 eV should nevertheless represent roughly the energy at both the third- and fourth-zone surfaces. Using the γ values given in table 1, we see that the density of states curve must look something like that shown in figure 13. The numbers of electrons and holes in the various zones are given by twice the areas under the curves and these numbers have been made to agree with those in table 1 by increasing the above estimates of E_0' a little. It is of course not possible to say anything about the form of this curve except in the immediate neighbourhood of the Fermi level.

(*b*) *Concluding remarks*

We have seen that it has been possible to build up a fairly detailed picture of the band structure near the Fermi level from the de Haas–van Alphen data, but there are some unsatisfactory features of the results which should be stressed. There are, in particular, four main experimental features which remain unexplained:

(i) The modulations in the envelopes of the α-oscillations which always appear to be in phase with the dominant γ-oscillations (p. 92).

(ii) The very large amplitudes of the β-oscillations near [100] and the dominant γ-oscillations near [110] (p. 106).

(iii) The unobservably small amplitudes of the γ-oscillations when the period falls below about $3{\cdot}7 \times 10^{-8}\,\text{G}^{-1}$ (pp. 97, 107).

(iv) The increase in period of the dominant γ-oscillations when lead is alloyed with small quantities of bismuth. This at first sight contradicts the proposed model by suggesting that the third- and fourth-zone surfaces contain holes and not electrons (p. 107).

These points have already been discussed in some detail and, although no convincing explanations have been found, they need not be regarded as necessarily being in conflict with the general interpretation of the results. The alternative interpretation discussed on p. 97, in which the fourth-zone is completely empty, cannot be rejected with complete certainty, but it seems most unlikely that it is true.

We note in conclusion that, although application of the free-electron model has served to relate the observed surfaces to the Brillouin zone scheme (and, indeed, to suggest the form of a multiply connected surface to account for what were at first rather perplexing results), the apparent likeness of the observed Fermi surface to the free-electron model is an aspect which should not, perhaps, be over-emphasized. Thus although the observed surfaces are of roughly the same size as the free-electron ones, the observed Fermi velocities are considerably lower than the free-electron value (table 1).

I should like to express my gratitude to Dr D. Shoenberg, F.R.S., for his helpful advice and encouragement and to Dr R. G. Chambers, Dr M. H. Cohen, Dr V. Heine and Dr A. B. Pippard, F.R.S., for many helpful discussions. My thanks are also due to Mr H. L. Davies for his help with the experiments and to Dr C. J. Ball for investigating the substructure in some crystals. I am indebted to the Carnegie Trust for a research scholarship and to the Department of Scientific and Industrial Research for a maintenance grant.

Note added in proof 14 *August* 1958. Lead is frequently divalent in chemical compounds ('inert pair') on account of the large $s-p$ splitting in the free atom. It therefore seemed worthwhile to examine a model for the metal in which the two s electrons are regarded as ion-core electrons and the two p electrons are 'tightly-bound' to the ions; the de Haas–van Alphen period data cannot be accounted for if the two p electrons are regarded as quasi-free. Energy matrix elements between states constructed from p-like atomic orbitals may be obtained from the 'tight-binding' interpolation scheme of Slater & Koster (1954) in terms of unspecified nearest-neighbour integrals $(pp\sigma)_1$ and $(pp\pi)_1$. Provided that $(pp\pi)_1$ is very much smaller than $(pp\sigma)_1$, solution of the secular determinant gives 'spherical' and multiply connected surfaces in two of the p bands, the third being empty; the Fermi level is chosen to make the dimensions of the surfaces agree as closely as possible with experiment. If we furthermore take second nearest neighbours into account and put $(pp\sigma)_2=\frac{1}{2}(pp\sigma)_1$, the three p bands become degenerate at W and we arrive at the same Fermi surface as proposed in table 1. The Fermi velocities (in certain directions) may be made to agree roughly with the averages in table 1 by putting $(pp\sigma)_1 \doteqdot 1$ eV. However the band structure is very sensitive to the value of $(pp\pi)_1$. Slater & Koster suggest that $|(pp\pi)_1|$ may be as large as $\frac{1}{3}(pp\sigma)_1$ but if $|(pp\pi)_1|>0{\cdot}1(pp\sigma)_1$ it is difficult to see how such a model can account for the proposed surfaces.

References

Berlincourt, T. G. 1952 *Phys. Rev.* **88**, 242.
Borovik, E. S. 1954 *J. Exp. Theor. Phys. U.S.S.R.* **27**, 355.
Bouckaert, L. P., Smoluchowski, R. & Wigner, E. 1936 *Phys. Rev.* **50**, 58.
Chambers, R. G. 1952 *Proc. Roy. Soc.* A, **215**, 481.
Chambers, R. G. 1956 *Canad. J. Phys.* **34**, 1395.
Dingle, R. B. 1952*a* *Proc. Roy. Soc.* A, **211**, 500.
Dingle, R. B. 1952*b* *Proc. Roy. Soc.* A, **211**, 517.
Dolecek, R. L. 1954 *Phys. Rev.* **94**, 540.
Elliott, R. J. 1954 *Phys. Rev.* **96**, 280.
Faber, T. E. & Pippard, A. B. 1955 *Proc. Roy. Soc.* A, **231**, 336.
Gold, A. V. 1957 *Proc. 5th Int. Conf. Low Temp. Phys. & Chem.* Madison.
Gunnersen, E. M. 1956 *Phil. Trans.* A, **249**, 299.
Heine, V. 1956 *Proc. Phys. Soc.* A, **69**, 505.
Heine, V. 1957 *Proc. Roy. Soc.* A, **240**, 340.
Lifshitz, I. M. & Kosevich, A. M. 1955 *J. Exp. Theor. Phys. U.S.S.R.* **29**, 730.
Lifshitz, I. M. & Pogorelov, A. V. 1954 *Dokl. Akad. Nauk. SSSR*, **96**, 1143.
Martius, U. M. 1954 *Progr. Metal Phys.* **5**, 295.
Meissner, W., Franz, H. & Westerhoff, H. 1932 *Ann. Phys., Lpz.*, **13**, 967.

PHILOSOPHICAL TRANSACTIONS OF THE ROYAL SOCIETY A MATHEMATICAL, PHYSICAL & ENGINEERING SCIENCES

Onsager, L. 1952 *Phil. Mag.* **43**, 1006.
Seitz, F. 1940 *Modern theory of solids.* New York: McGraw-Hill Book Co.
Shoenberg, D. 1952 *Phil. Trans.* A, **245**, 1.
Shoenberg, D. 1953 *Physica*, **19**, 791.
Shoenberg, D. 1957 *Progr. Low Temp. Phys.* **2**, 226.
Slater, J. C. & Koster, G. F. 1954 *Phys. Rev.* **94**, 1498.
Solomon, D. & Morris-Jones, W. 1931 *Phil. Mag.* **11**, 1090.
Tiller, W. A. 1957 *J. Metals*, **9**, 847.
Zilberman, G. E. 1956 *J. Exp. Theor. Phys. U.S.S.R.* **30**, 1092.
Zilberman, G. E. 1957 *J. Exp. Theor. Phys. U.S.S.R.* **33**, 387.

PHILOSOPHICAL TRANSACTIONS OF THE ROYAL SOCIETY A MATHEMATICAL, PHYSICAL & ENGINEERING SCIENCES

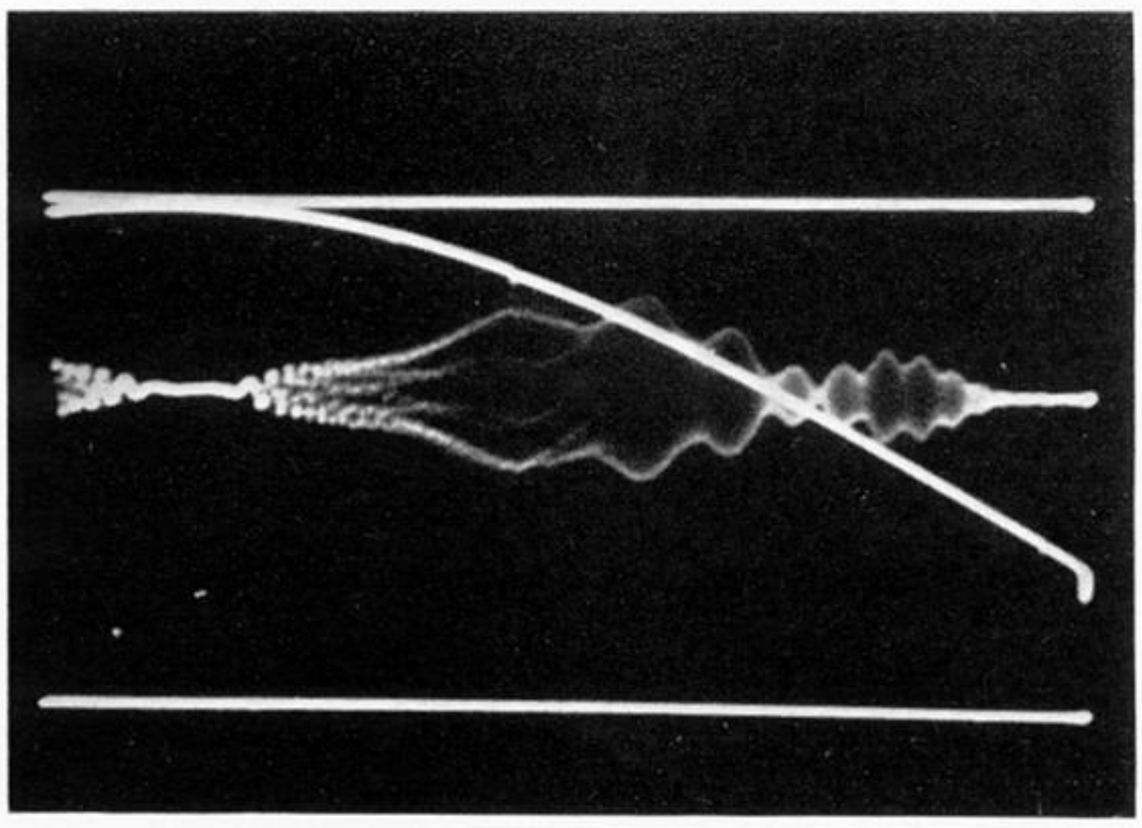

a

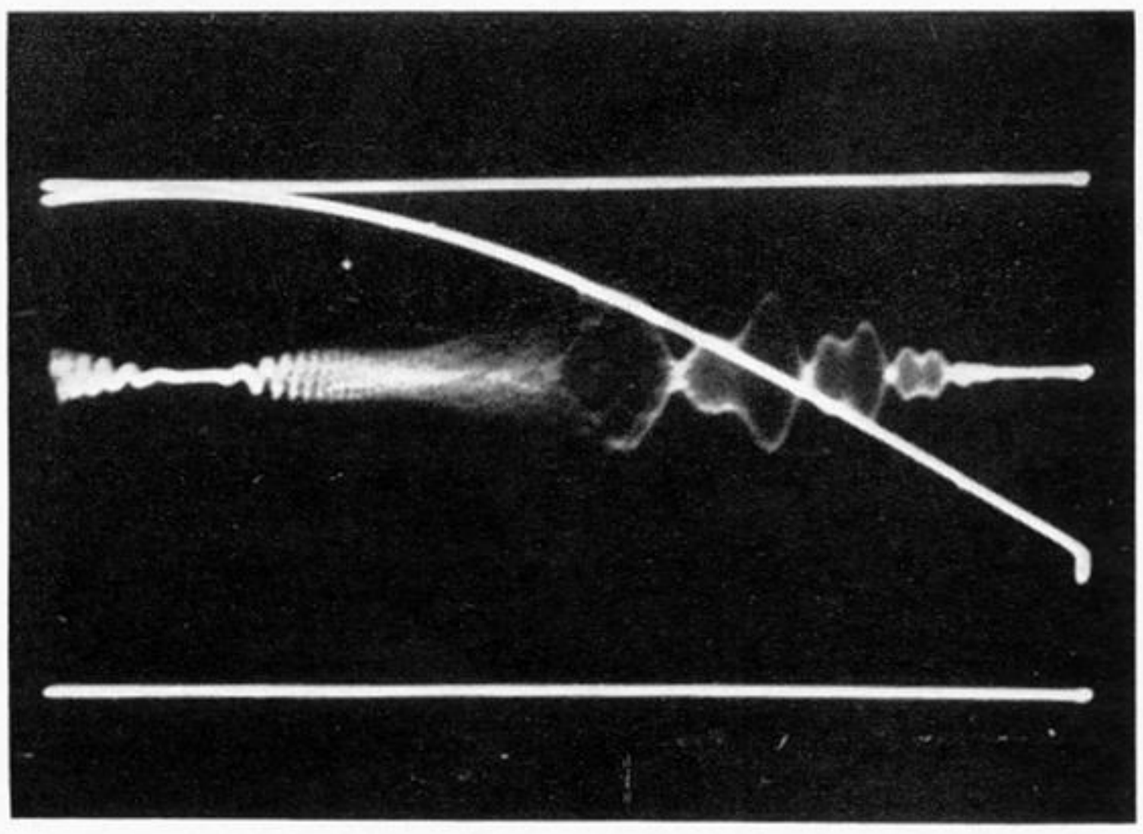

b

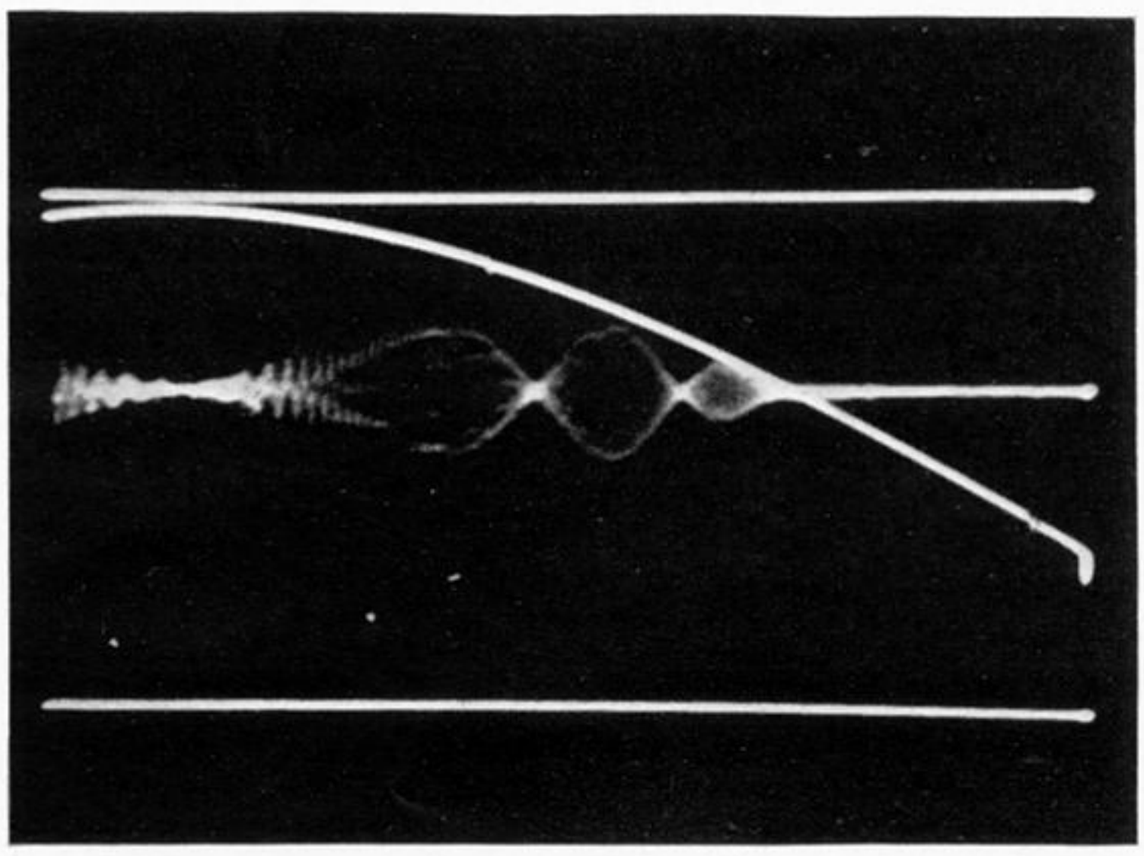

c

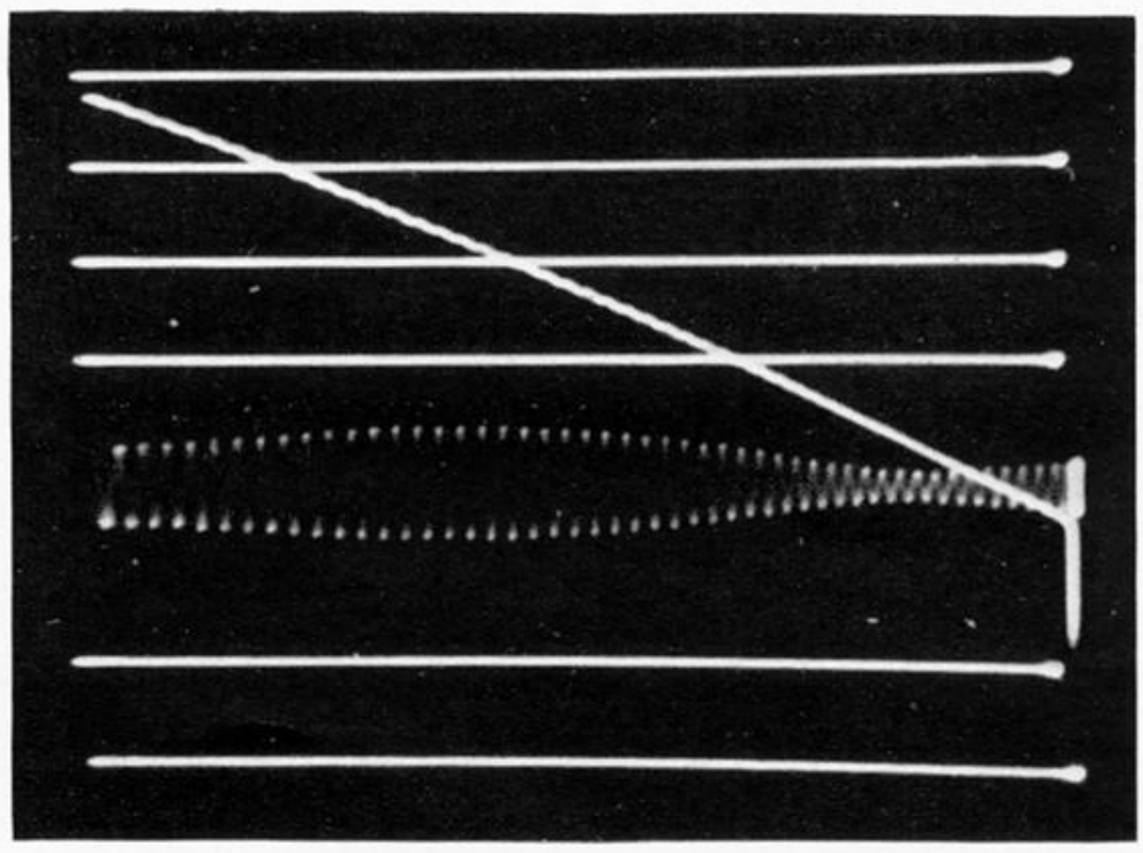

d

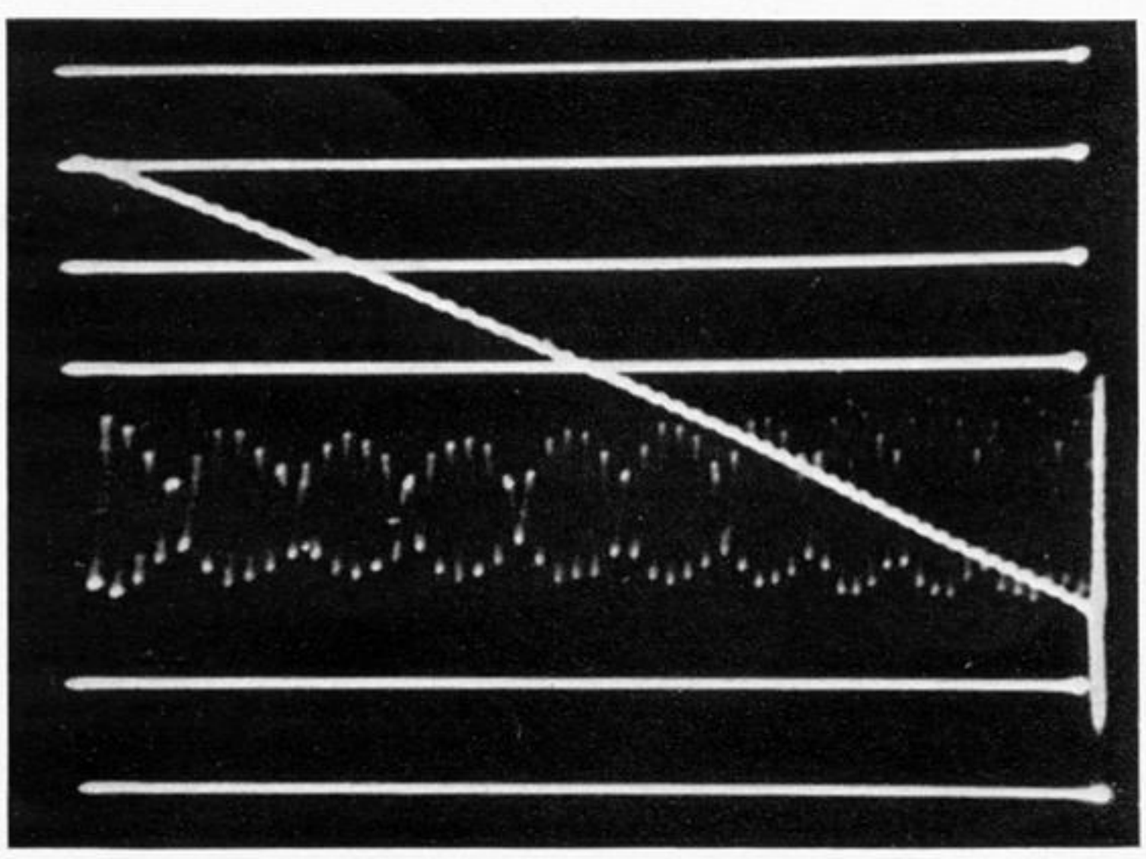

e

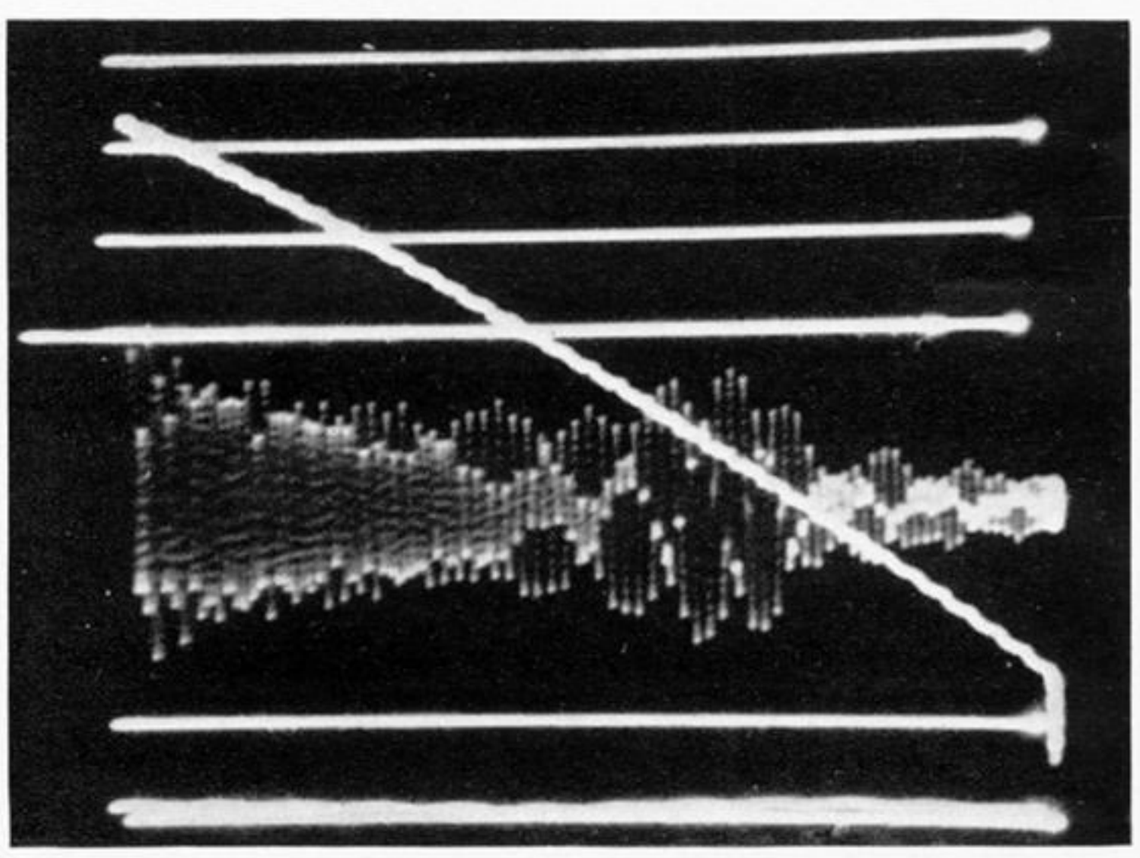

f

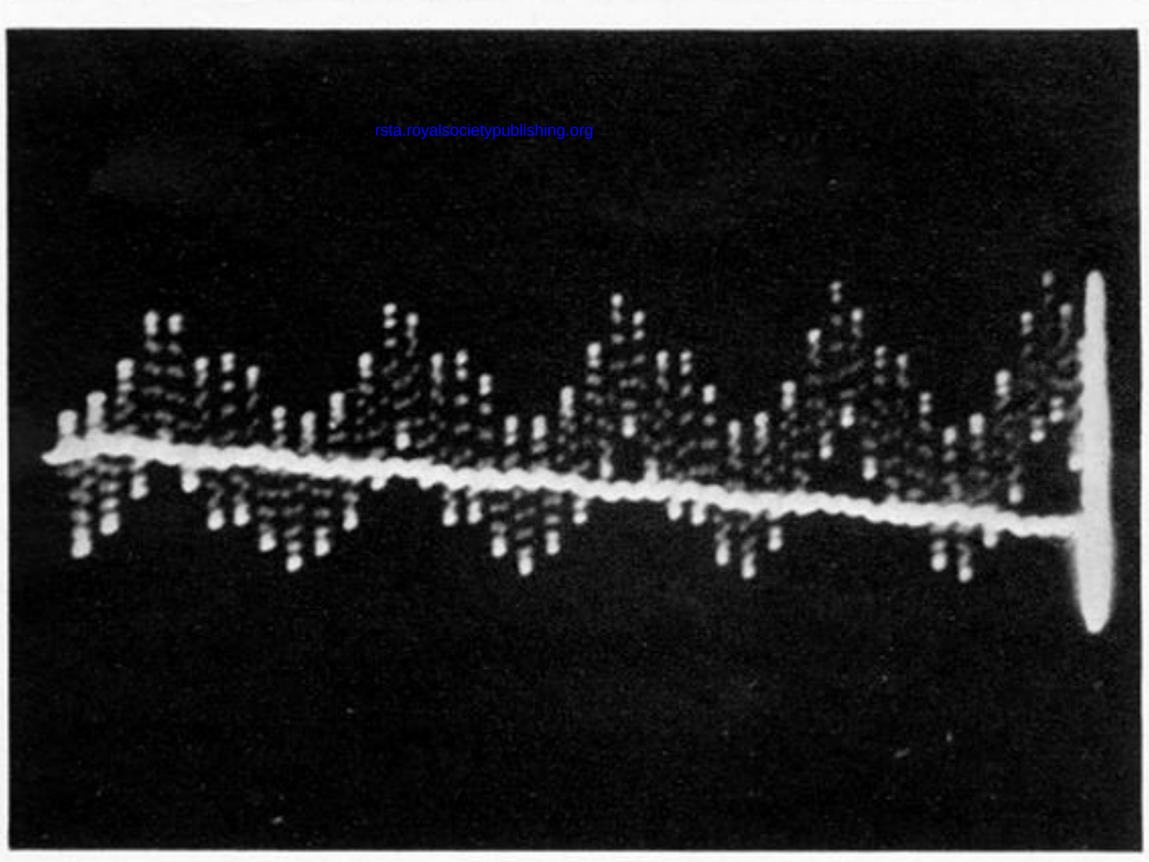

g

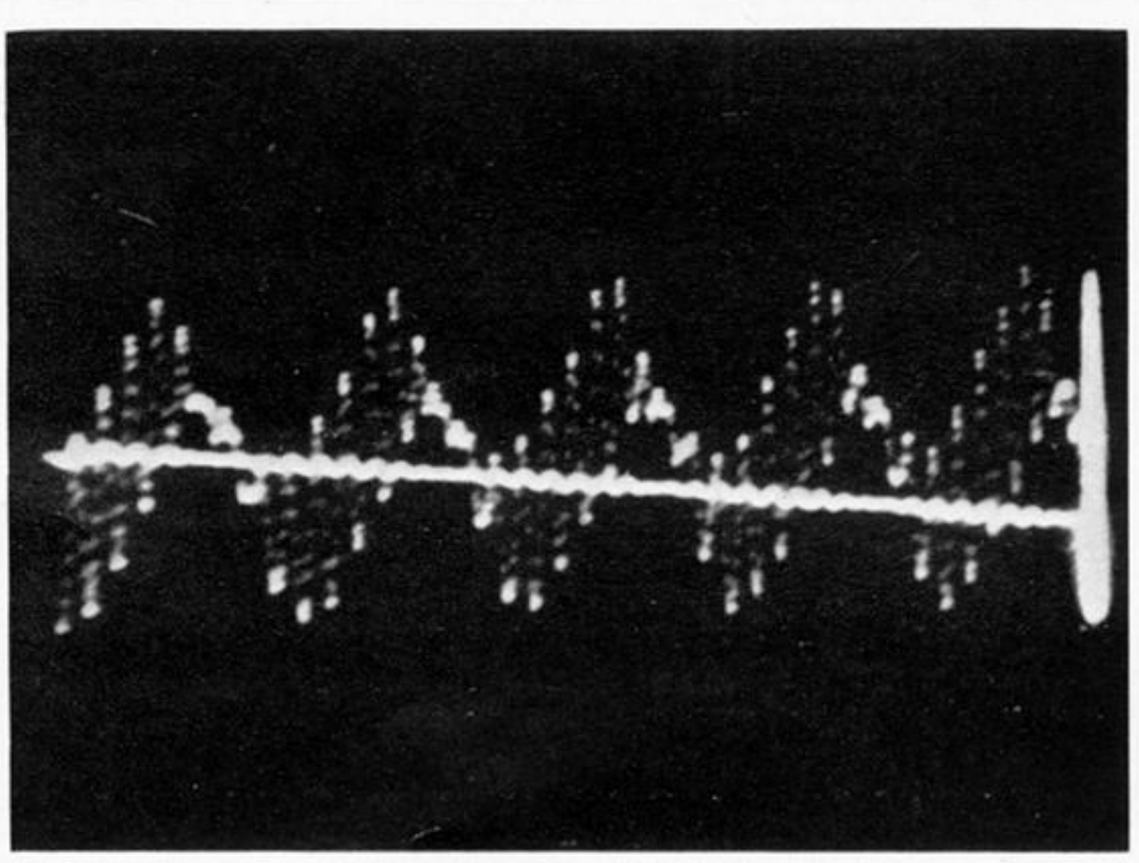

h

IGURE 1. Typical oscillograms of lead oscillations. *a*, *b* and *c* are envelope pictures of the γ-oscillations at 30°, 40° and 45° from [100] in a (100) plane (i.e. *c* is at [110]). $T = 2{\cdot}3\,^{\circ}\mathrm{K}$; at $T = 1{\cdot}2\,^{\circ}\mathrm{K}$ the patterns extend to lower fields so that, for example, three more beats are observed at [110]. *a*, *b* and *c* show the field variation directly without using the 'back-off' technique; the sweep time is 15 ms and the horizontal calibration lines correspond to 0 and 80 kG. The remaining oscillograms are expanded pictures with sweep times from 0·5 to 1·5 ms. *d* and *e* show the γ-oscillations at two different orientations and *f* illustrates a resonance of group γ against a background of group β (at [100]); the calibration lines are at intervals of 1·57 kG and the baselines correspond to 44, 44 and 52 kG for *d*, *e* and *f*, respectively. *g* and *h* show the α-oscillations superimposed on the slower γ ones.

(*Facing p.* 88)